CONTEMP. PHYS., 1986, VOL. 27, NO. 5, 395–428

The electron–hole liquid in semiconductors†

L. V. Keldysh, P.N. Lebedev Physical Institute of the Academy of Sciences, Moscow 117924, U.S.S.R.

ABSTRACT. In highly excited semiconductors at low enough temperatures nonequilibrium electrons, holes and excitons condense into droplets of a metallic degenerate Fermi liquid, the so called electron–hole liquid. General properties of this new quantum liquid are reviewed including possible types of its phase diagram; the strong dependence of the phase diagram on the band and crystalline structure of the semiconductor, magnetic field etc.; the kinetics of electron–hole drop nucleation, growth and decay. Electron–hole drops can easily be accelerated by some external forces up to velocities close to that of sound. Intense movement of drops also occurs because of the so called phonon wind-drag by intense flows of nonequilibrium phonons, arising in recombination processes inside the drops themselves or in the thermalization of excited carriers.

1. Introduction

In quantum many-body theory the usual way of describing a macroscopic system is in terms of elementary excitations such as phonons, magnons, electrons and holes, etc., above some ground state. The convenience and usefulness of the elementary excitation concept itself are obvious if the excitation interaction is negligible or small enough compared to its energy, and the system of elementary excitations can be treated as a gas. It fails, however, in the vicinity of second-order phase transitions, where for some group of elementary excitations the interaction becomes strong, resulting in sharp changes in the nature of the excited states and of the corresponding physical properties. Similar conditions can be achieved far from equilibrium if some excitation modes are intensely pumped and the number of elementary excitations in these modes becomes large enough. Condensation of nonequilibrium charge carriers in semiconductors into the metallic degenerate Fermi liquid of electrons and holes is today one of the best-studied examples of this phase transition far from equilibrium. Arising in highly excited semiconductors, the electron–hole liquid (EHL) has been the subject of numerous theoretical and experimental investigations for the last fifteen years and the results of this work are summarized in several reviews [1–9]. In this article the presentation partially follows that in [9].

2. Interaction and bound states in the system of nonequilibrium charge carriers

In the case of semiconductors the so-called free charge carriers, electrons and holes, are the most important type of elementary excitations. At distances much larger than that between atoms they interact via the usual Coulomb forces, reduced by dielectric screening,

$$V(r_{12})=\frac{e_1e_2}{\varepsilon r_{12}}. \tag{1}$$

Here V is the potential energy of two point charges, e_1 and e_2, and r_{12} is the distance between them. The overwhelming majority of the phenomena in the physics of

† This article is based on the paper Electron–Hole Droplets in Semiconductors (from *Modern Problems of Condensed Matter Sciences*, Vol. 6, 1983, pp. xi-xxxvii, published by Elsevier North-Holland) and includes material from a lecture presented at the Enrico Fermi Summer School, 1983, which subsequently appeared in *Nuovo cimento* (Italian Physical Society). Permission to use this material is gratefully acknowledged.

semiconductors can be understood in terms of free charge carriers, neglecting their interaction, because usually this interaction is small compared to the thermal kinetic energy $k_B T$ if the temperature T is not too low and the concentration of electrons and holes n is not too large:

$$\frac{e^2}{\varepsilon |\mathbf{r}|} \sim \frac{e^2}{\varepsilon} n^{1/3} \ll k_B T. \tag{2}$$

The values of the dielectric constant ε for semiconductors are typically large, $\varepsilon \gtrsim 10$, and it is one of the most important properties determining the usefulness of the free-charge-carrier concept itself. For $T \sim 100\,\mathrm{K}$ the inequality (2) is fulfilled at all concentrations up to $n \sim 10^{18}\,\mathrm{cm}^{-3}$. The problem to be considered here is what happens to the system of free charge carriers if the temperature is low enough and the charge carrier density is high enough, so that the above-mentioned inequality is violated and the interaction becomes strong.

The conditions of high concentration and low temperature are incompatible in intrinsic (pure enough) semiconductors at thermodynamic equilibrium. In this case

$$n \sim \left(\frac{m k_B T}{\hbar^2}\right)^{3/2} \exp\left[-\frac{E_g}{2 k_B T}\right] \tag{3}$$

and, as the temperature decreases, decreases much faster than the temperature itself (E_g is the energy gap, i.e. the minimum energy necessary to produce one electron–hole pair). But concentration can be made arbitrarily large at any temperature, under non-equilibrium conditions, when additional electron–hole pairs are artificially produced by some external source (illumination, injection through contacts and so on). In this sense the subject of this article is a system of nonequilibrium charge carriers at low temperatures. However, the nonequilibrium nature of this system will be understood here in some restricted sense. The reason is that there exist two very different time scales in the problem under consideration: the thermalization time τ and the recombination time (nonequilibrium charge carrier lifetime) $\tau_0 \gg \tau$. This means that charge carriers, initially produced with kinetic energies much larger than $k_B T$, thermalize very fast, i.e. acquire a nearly equilibrium energy distribution corresponding to the crystal lattice temperature. But after that they exist for much longer time intervals in such a quasi-equilibrium state, and the only nonequilibrium parameter is the total number of carriers, which is fixed at an arbitrary value by the external excitation source and does not correspond to formula (3). In this sense the nonequilibrium charge carrier system will be treated approximately in what follows as an equilibrium system of electrons and holes, but with an arbitrarily fixed total number of particles. Some of its unusual properties arising only from the nonequilibrium nature of the system will be described in the last section of this paper. One of the best known manifestations of the Coulomb interaction between electrons and holes is the existence of Wannier–Mott excitons, bound states of the electron and hole, similar to the hydrogen atom and positronium. The resemblance of the Wannier–Mott exciton to the positronium is closer than that to the hydrogen atom for two reasons: unlike the electron and the proton, the effective mass values of the electron and hole in semiconductors differ usually by no more than one order of magnitude, and the lifetime of the exciton is finite owing to the possible recombination of the electron and the hole. But quantitatively excitons differ

drastically from both the hydrogen atom and positronium. Evaluated by the well-known Bohr formulae the exciton binding energy E_{ex} and the effective radius a_{ex} are

$$E_{ex}=\frac{1}{2}\frac{e^4m}{\varepsilon^2\hbar^2}\sim(10^{-1}-10^{-3})\text{eV}, \tag{4a}$$

$$a_{ex}=\frac{\varepsilon\hbar^2}{me^2}\sim(10^{-6}-10^{-7})\text{cm}, \tag{4b}$$

where e, $\hbar$ and m are respectively the electronic charge, Planck's constant and the reduced effective mass of the electron and hole. They differ from the Rydberg and the Bohr radius by several orders of magnitude because of the above-mentioned large values of the dielectric constant and the relatively small values of m, which are usually smaller by an order of magnitude than the free electron mass. One important consequence of these numerical estimates, which is fundamental to the whole of the following discussion of the properties of the interacting charge carrier system and to the validity of equations (4) themselves, should now be explained. Values of a_{ex} which are large compared to interatomic distances in the host crystal justify not only the applicability to the problem of excitons of the interaction law in the Coulomb form (1), but also the possibility of treating this problem as that of two particles interacting in a spatially homogenous effective medium, i.e. ignoring details of the real crystal structure and crystal potential, which manifest themselves only indirectly in the values of effective mass and dielectric constant. Because the values of E_{ex} are small compared to the binding energies of atoms and valence electrons, even at such high concentrations as will be discussed later, the interaction of free charge carriers, including exciton formation, does not noticeably influence the host crystal structure, its bound electron and phonon spectra etc. In other words, within some approximation, free charge carriers and excitons constitute an autonomous subsystem for which the host crystal represents a neutral spatially uniform background, some kind of vacuum determining the energy spectrum of carriers (effective masses) and their interaction (dielectric constant). The evolution of the properties of this subsystem, depending on the temperature T and the concentration n, may be understood from simple qualitative considerations, based on the following observations:

(1) It is, as a whole, an electroneutral assembly of many oppositely charged particles, interacting according to the Coulomb law (1) and, therefore, analogous to a system of electrons and nuclei (protons, for example). The values E_{ex} and a_{ex} (4) for this system are the natural quantum scales of energy and length in the same way as the Rydberg and the Bohr radius are the natural scales of energy and length in atoms, molecules and solids, because no other quantities of energy and length dimension can be constructed from e^2/ε, $\hbar$ and m—the only intrinsic dimensional parameters entering the dynamics of the system under consideration.

(2) The most fundamental qualitative difference of the electron–hole system from that of the electron–proton system is the absence of heavy particles in the former, since the effective masses of electrons m_e and holes m_h are usually of the same order of magnitude. Therefore, the adiabatic approximation—one of the most fruitful concepts in molecular and solid-state physics—is not valid in our problem because its accuracy is $(m_e/m_h)^{1/4}$.

At high temperatures and low enough concentrations, when

$$n \ll \left(\frac{mk_B T}{\hbar^2}\right)^{3/2} \exp\left[-\frac{E_{ex}}{2k_B T}\right], \tag{5}$$

the free-charge-carrier system is nearly a perfect gas or, more correctly, nearly a perfect completely ionized plasma. Exciton concentration is negligibly small, owing to the thermal dissociation, and interaction is weak as inequality (2) is automatically fulfilled. The system also remains nearly perfect even at arbitrarily low temperature if the concentration is large enough, $na_{ex}^3 \gg 1$, but in this case the system is a degenerate plasma, and the interaction is weak compared to its Fermi energy. In the intermediate concentration range

$$\left(\frac{mk_B T}{\hbar^2}\right)^{3/2} \exp\left[-\frac{E_{ex}}{2k_B T}\right] \lesssim n \lesssim a_{ex}^{-3}, \tag{6}$$

which exists apparently only at low temperatures where $k_B T \lesssim E_{ex}$, the interaction becomes strong and its influence on the system properties dominating. This is the range of nontrivial states of the system and the main subject of the following discussion.

If the concentration is not large, $na_{ex}^3 \ll 1$, then as the temperature decreases, violating inequality (5), the majority of electrons and holes combine into excitons. Recalling the above-mentioned analogy of excitons to atoms, we can treat this state of the nonequilibrium charge carrier system as an atomic gas or a weakly ionized plasma. Proceeding with this analogy, one can expect at still lower temperatures the formation of excitonic molecules, biexcitons, proposed initially by Moskalenko [10] and Lampert [11]. The existence of biexcitons is established with certainty now, both theoretically and experimentally [12, 13], but, unlike excitons, which differ from hydrogen atoms only quantitatively, they differ qualitatively from hydrogen molecules in some respects. The reason for this difference, very important for the following analysis of the strongly interacting electron–hole system, is the above-mentioned absence of the adiabaticity in the electron–hole problem. For this reason in biexcitons, unlike the hydrogen molecule, not only the electrons but also the holes are strongly delocalized, which results, as will be shown now, in a sharp reduction of the molecular binding (dissociation) energy E_D.

In figure 1 the usual interaction potential of two hydrogen atoms in the singlet state is shown schematically. It would be essentially the same for excitons if $m_e \ll m_h$ and the natural quantum scales a_{ex} and E_{ex} are used instead of the usual atomic Bohr radius and Rydberg. The dissociation energy differs from the potential well depth U_0 by a small amount, equal to the zero-vibration energy $\frac{1}{2}\hbar\omega_0 \sim (m/M)^{1/2} U_0$. Here m and M are electron and proton masses. If it were possible to reduce smoothly the heavy particle mass M, the ground-state energy level would shift upwards, as shown in figure 1, due to the increase of zero-point vibration amplitude and energy. For this reason the relative contribution of zero-point vibrations to the total biexciton energy is greater by more than an order of magnitude than in the molecule H_2 and almost completely compensates the adiabatic attractive potential. For a difference of electron and hole masses within one order of magnitude, such qualitative estimates give $E_D \lesssim 0{\cdot}1\ E_{ex}$ for the biexciton dissociation energy. This value is confirmed both by more accurate variational estimates and by the available experimental data [12, 13]. For hydrogen the ratio of the molecular dissociation energy to the atomic binding energy is 0·35. Since $(m_e/m_h)^{1/4}$ is

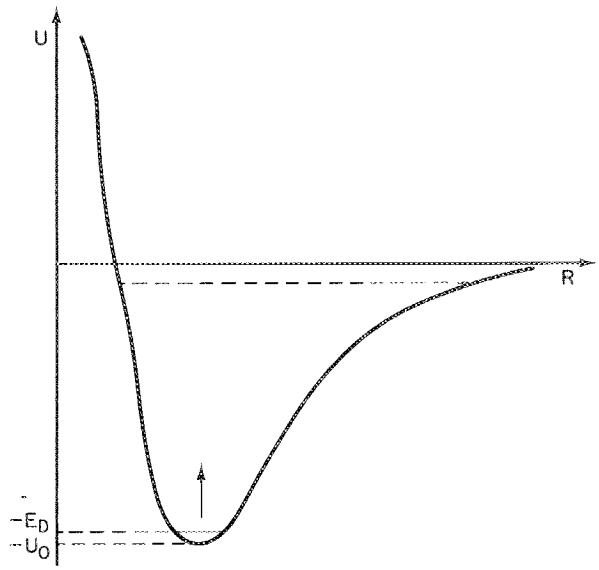

Figure 1. Interaction potential of two excitons in reduced 'excitonic' units (E_{ex}, a_{ex}). The arrow indicates the direction of the ground-state energy level shift as the electron to hole mass ratio changes from 0 to 1.

always of the order of unity, the zero-point vibration amplitude in a biexciton is of the order of a_{ex} and probably even larger since the dissociation energy is so small. Thus holes are indeed completely delocalized inside the excitonic molecule and this molecule is a very loosely bound system.

So, at low enough temperatures and concentration, fulfilling the condition (6), the nonequilibrium electron–hole system exists in the form of a gas of excitons, biexcitons and free charge carriers. According to the same analogy of electron–hole and electron–nuclei systems one would expect that, at still lower temperature or higher concentration (gas pressure), the nonequilibrium electron–hole system would undergo something like a gas–liquid phase transition, accompanied by the formation of some condensed phase (liquid) of nonequilibrium charge carriers [14]. The word 'liquid' is used here in its usual meaning: a system of a macroscopically large number of particles occupying a macroscopically large volume and bound together by internal interaction forces. It is characterized by a definite equilibrium density (concentration of electron–hole pairs) n_l, binding energy (work function) per electron–hole pair E_l and surface tension, i.e. the capacity to form a sharp, stable boundary, separating it from the gas phase. Contrary to the usual behaviour of the electron–hole plasma or the exciton gas, it does not tend to spread over the whole crystal volume, but occupies only a definite part of it, $V_l = N_l/n_l$, where N_l is the total number of particles in this phase. But sharing these general features with any other known liquid, the electron–hole liquid (EHL) is unique in many other properties, which will be described below.

In this article the modern status of EHL study and understanding will be briefly presented, illustrated by a few experimental and theoretical results. Comprehensive review of the subject, including full lists of references, may be found in the monographs [7–9].

3. Thermodynamics of the electron–hole liquid

3.1. *The electron–hole liquid: qualitative description*

In this section, the main properties and manifestations and the existence region of the EHL in different types of semiconductor will be discussed under the assumption of thermodynamic equilibrium within the charge carrier system, i.e. neglecting the electron–hole recombination process, which, as explained above, is a good starting approximation. In this case the considerations in the preceding section may be conveniently illustrated and essentially supplemented by a schematic phase diagram (figure 2) on the plane of variables $(T, \bar{n})$. Here T is the temperature, and $\bar{n}$ is the mean concentration of electron–hole pairs: $\bar{n}=N/V$. N is the total number of pairs and V the volume of the excited region, which for simplicity is considered to be uniformly excited. In figure 2 as a scale of temperature and concentration their values are used at the spatially uniform gaseous and liquid phases of the nonequilibrium carrier system. The shaded region G+L is that of the parameter values where the spatially uniform distribution appears to be unstable and there occurs separation into liquid-phase droplets with equilibrium density $n_l(T)$, surrounded by exciton, biexciton and free-carrier gas with equilibrium density $n_g(T)$. Here $n_l(T)$ and $n_g(T)$ are correspondingly the right and left branches of the curve limiting the region of phase coexistence in figure 2. In figure 2 as a scale of temperature and concentration their values are used at the so-called critical point (T_c, n_c), i.e. at the point at which the difference between gas and liquid disappears. At $T/T_c>1$ there is no density at which the phase transition occurs, i.e. the nonequilibrium carrier concentration increases continuously with increase of excitation level. The value T_c is likely to be determined by the particle binding energy in the condensed phase E_l. There exists the well-known empirical correlation $k_B T_c \approx 0{\cdot}1\, E_l$ [15] valid for many liquids as well as for the nonequilibrium carrier liquid phase in semiconductors. According to the above consideration of energy and length scales in the nonequilibrium carrier system the orders of magnitude of the main parameters of the condensed-phase and its existence region may be estimated: $n_c \sim n_l \sim a_{ex}^{-3}$, $10 k_B T_c \sim E_l \sim E_{ex}$, i.e. the mean interparticle distance in the condensed phase should be of the order of a_{ex} and the binding energy per electron–hole pair of the order of E_{ex}.

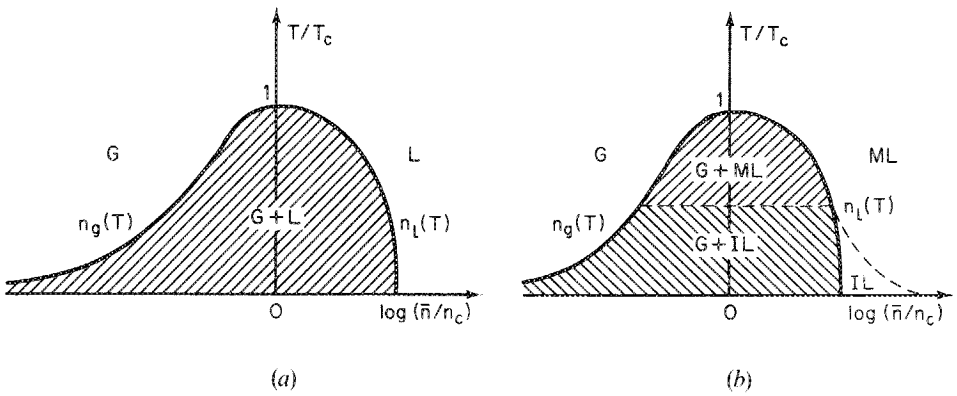

Figure 2. Possible types of nonequilibrium charge carrier system phase diagrams. The letters G and L denote the existence region of spatially uniform gas and liquid states ; ML and IL metallic liquid and insulating liquid. The coexistence region of electron–hole droplets and gas is hatched.

Let us now discuss the structure and the main physical properties of the condensed phase. At this stage the above-mentioned fundamental difference between the nonequilibrium carrier system and that of the electron and nuclei system, that is, the absence of heavy particles, acquires decisive significance. Because of this there is no temperature at which crystallization, i.e. the formation of a 'solid' phase in the nonequilibrium carrier system, is possible. Essentially, because $(m_e/m_h)^{1/4}$ is not a small parameter, there is no length dimension scale, except a_{ex}. Therefore, if crystallization occurred, the particle zero-vibration amplitude around the equilibrium positions would be of the order of a_{ex}, that is of the order of interparticle distances, and this, according to existing melting criteria, should already result in melting at zero temperature. Hence the non-equilibrium carrier condensed phase is a liquid with extreme quantum properties. However, there exist liquids very different in structure and properties: molecular, metallic, ionic (electrolytes), and so on. Proceeding from the exciton analogy to hydrogen atoms, one might suppose that the nonequilibrium carrier condensed phase is a molecular liquid of biexcitons, weakly bound with each other. However, this is not correct, and the analogy itself at this point is not unambiguous. Indeed, the closest analogues to hydrogen, the alkali metals, condense not into molecular but into metallic liquids. The reason for this qualitative difference is a considerable difference in binding (dissociation) energy E_D of the corresponding molecules. The strongly bound ($E_D \approx 0{\cdot}35$ Ryd) molecule H_2 with a completely saturated valence bond and, therefore, interacting with other surrounding molecules only via weak Van der Waals forces, appears to be stable and energetically the most favourable structural unit in the liquid phase. Intermolecular distances here exceed essentially interatomic distances within a molecule, and the interaction of each atom with its partner within the same molecule exceeds by several orders of magnitude its interaction with neighbouring molecules. The molecules Na_2, K_2, Cs_2, etc. ($E_D < 0{\cdot}1$ Ryd) which are much more loosely bound owing to the presence of filled electron shells, do not survive in the condensed phase. Intramolecular binding is not strong enough to provide an energy advantage for a liquid whose components are molecular rather than atomic, where each atom would interact strongly with a few nearest, approximately equidistant, neighbours. In this latter case an intense electron exchange among all nearest neighbours results in complete electron delocalization, i.e. in the formation of a metallic liquid.

The exciton binding in the excitonic molecule is also rather weak, as explained above, owing to the absence of heavy nuclei and the correspondingly large zero-point vibration amplitude. Moreover, large zero-point vibration amplitudes not only weaken the intramolecular bond but, in addition, if molecules existed in the liquid phase, these large zero point vibrations would greatly increase the overlap of the wavefunctions of excitons in neighbouring molecules and the electron exchange between them. As a result, the condensed phase in the charge carrier system in semiconductors cannot be a molecular liquid. Like liquid alkali metals it is a metallic liquid, where neither excitonic molecules nor excitons themselves are present [14]. Electrons and holes in this electron–hole liquid (EHL) are 'free' in the same sense as electrons are free in metals: they move freely and more or less independently of each other (without violating macroscopic electroneutrality) within the liquid volume, but they cannot leave it, unless they are supplied with additional energy exceeding the so-called work function. The main qualitative difference of the EHL from ordinary metals is the complete quantum delocalization of both electrons and holes. From the above-mentioned estimates of the main condensed-phase parameters, the temperature of Fermi

is and the existence region of
ssed under the assumption of
system, i.e. neglecting the
ed above, is a good starting
preceding section may be
a schematic phase diagram
nperature, and $\bar{n}$ is the mean
al number of pairs and V the
lered to be uniformly excited.
their values are used at the
uilibrium carrier system. The
where the spatially uniform
eparation into liquid-phase
exciton, biexciton and free-
$i_g(T)$ are correspondingly the
phase coexistence in figure 2.
their values are used at the
e difference between gas and
the phase transition occurs,
ntinuously with increase of
he particle binding energy in
rical correlation $k_B T_c \approx 0{\cdot}1\, E_l$
rium carrier liquid phase in
f energy and length scales in
le of the main parameters of
be estimated: $n_c \sim n_l \sim a_{ex}^{-3}$,
condensed phase should be
ole pair of the order of E_{ex}.

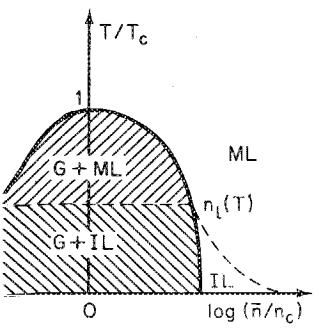

(*b*)

phase diagrams. The letters G
and liquid states ; ML and IL
n of electron–hole droplets and

degeneracy T_F of the carriers in it is

$$k_B T_F \sim \frac{\hbar^2}{m} n_l^{2/3} \sim \frac{\hbar^2}{m a_{ex}^2} = 2E_{ex} \gtrsim k_B T.$$

so throughout the whole domain of its existence the EHL is a degenerate two-component Fermi liquid.

Within this general picture the EHL parameters and properties in different semiconductors and under different experimental conditions can be rather diverse. They are extremely sensitive to the peculiarities of the electron spectrum of the semiconductor and to any external influence. In those semiconductors where the electron and hole masses differ by an order of magnitude or more the heavy carriers may appear to be nondegenerate at temperatures of the order of the critical one. In these semiconductors the spatial correlation (short-range order) in the heavy-carrier arrangement already resembles the short-range order in the ion arrangement in molten metals, but still shows pronounced quantum effects, especially at $T \ll T_c$. To produce a crystal with long-range order, even at $T = 0$, a difference in carrier effective mass of more than two orders of magnitude is necessary [16], which is unlikely in intrinsic semiconductors. Still more essential is band degeneracy and, especially, the so-called multivalley band structure, i.e. the presence (due to crystal symmetry) of several equivalent electron or hole groups, or both. Such are the band structures of many well-known semiconductors: Ge, Si, C, GaP, $A^{IV}B^{VI}$ group compounds, etc. It appears that in this case, n_l, E_l and T_c are much greater than they would be in semiconductors with the same effective-mass values and dielectric constant, but with the simple single-valley spectrum both for electrons and holes. The origin of this phenomenon is not difficult to explain qualitatively [17]. The particle energy in the EHL is composed of kinetic (Fermi) energy, which is positive, and potential energy from the Coulomb interaction, which is essentially negative, because due to the correlation in particle movement each particle is surrounded mainly by oppositely charged particles. The equilibrium density is determined by the minimum condition for total energy, i.e. by some balance of these two contributions, as shown in figure 3. A transition from the single-valley to the multivalley case at a fixed concentration would disturb this balance, as the Fermi energy, determined by the number of particles in each valley, would be essentially

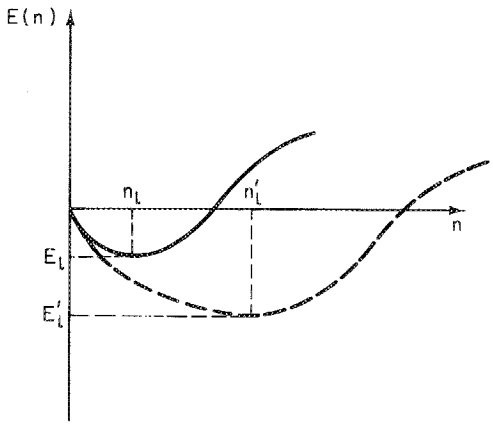

Figure 3. Concentration dependence of the EHL energy E_l in single valley (full line) and multivalley (dashed line) cases.

reduced, while the potential energy dependent in a first approximation only on the mean distance between the particles, i.e. on their total concentration, would be virtually unchanged. The disturbed balance would result in a spontaneous contraction of the system to such a concentration that the growth in the Fermi energy would compensate any further increase in potential energy. Thus both concentration and binding energy are much greater in the new equilibrium position than in the initial one, corresponding to the single-valley band structure (figure 3), i.e. the multivalley band structure considerably increases the EHL stability and the range of its existence in the plane of the variables (n, T). The exciton binding energy does not depend on the number of valleys, since the electron and hole which comprise the exciton each belong to only one of the corresponding valleys. In the same direction and for similar reasons the EHL stability is also enhanced if the effective masses are strongly anisotropic. Indeed, the Fermi energy depends on the density of states, i.e. on the so-called density-of-states effective mass $m_d = (m_1 m_1 m_3)^{1/3}$, where m_i are the principal values of the effective mass tensor: the relationship $E_F = (\pi^2\hbar^2/2m_d)(3/\pi n)^{2/3}$. Thus, if, starting from the isotropic case $m_{1,2,3} = m$, one of the masses, e.g. m_1, increased, at a fixed concentration n, then E_F would evidently decrease $\sim(m/m_1)^{1/3}$. In the same way as in the multivalley case, the decrease in E_F results in an increase in equilibrium density and EHL binding energy. At the same time, the mean distance between particles in an exciton is mainly determined by the smallest of the masses, since, in the case of anisotropic masses, the exciton is elongated in the direction in which the quantum delocalization effect is most strongly pronounced, i.e. in the smallest mass direction. Even at $m_1 \to \infty$, a_{ex} diminishes only by a factor of two, E_{ex} correspondingly increases four-fold, while E_1 grows as $(m_1/m)^{1/5}$.

Such external actions as uniaxial stress or magnetic field, lowering the crystal symmetry, destroy the valley equivalence, so electrons (holes) remain only in some of them if the action is strong enough. Choosing a different stress or field direction, one can produce a different number of equivalent valleys in the same semiconductor and so it is possible to change the EHL parameters within wide limits.

Intervalley electron transitions are comparatively rare. Therefore, in discussing the EHL structure, electrons (holes) from different valleys may be approximately considered to be different types of particles. From this standpoint, the EHL in multivalley semiconductors is a multicomponent Fermi liquid, and external actions make it possible to change the number of its components or their relative concentrations arbitrarily. In certain cases these changes occur via a first-order phase transition [18], which is easy to understand on the basis of the above discussion of the increase in binding-energy in the multivalley case. The possibility of varying all the main EHL parameters within wide limits enables us to observe many new physical phenomena and makes the EHL an ideal model for studying collective phenomena in multielectron systems.

Compared to all known liquid, the EHL has the least mass density, $(m_e + m_h)n_1 \sim m a_{ex}^{-3} \sim (10^{-6}\text{–}10^{-8})\,\mathrm{kg\,m^{-3}}$. Together with the small binding energy this is also the cause of its extreme sensitivity to any external influence: electric and magnetic fields, crystal deformation, and so on. In particular, the liquid is easily accelerated and flows inside the crystal. One should bear in mind, however, that, owing to electric neutrality, this flow is accompanied neither by an electrical current nor by any transfer of matter. As a hole represents the absence of an electron, an electron–hole pair has an effective mass, but not a real one (with a precision of $E_g/c^2 \sim 10^{-36}$ kg, where E_g is the energy gap width in the semiconductor in question and c is the light velocity). The above-estimated mass density is the *effective* mass density, which determines the

EHL inertial properties and its response to external forces, but does not describe the matter content. Like the exciton, which is essentially the excitation energy quantum in a crystal, the EHL is spatially condensed excitation energy with density $n_1 E_g \sim 10^6\ \mathrm{J\,m^{-3}}$, and its flow is first of all a transfer of excitation energy. This energy drastically changes the crystal properties, transforming it into a new phase state. In the region where it is concentrated, n_1 of the interatomic bonds per unit volume are broken, and the n_1 electron–hole pairs thus formed are in a metallic Fermi liquid state as described above.

These transformations are especially spectacular at excitation levels and temperatures corresponding to the G+L region in the phase diagram of figure 2. In this parameter region the EHL exists as macroscopic droplets—the so-called electron–hole drops (EHD).

According to the above considerations, EHD are mobile semimetallic phase regions inside insulating crystals, while from another point of view they are stable bunches of excitation energy. EHD motion is transfer of excitation energy as well as that of metallic conductivity and all other EHL properties. The ability to move freely inside a crystal without damaging it is one of the most remarkable features of EHD, distinguishing it from other macroscopic objects and emphasizing its quantum nature.

3.2. *Theory of the electron–hole Fermi liquid*

The central problem of EHL theory is finding the dependence of the EHL phase diagram parameters on electron and hole spectra and other semiconductor characteristics. Two main parameters—the dielectric constant and some mean electron and hole mass—determine the effective Bohr radius and Rydberg, i.e. the scales along the n and T axes in the phase diagram. In addition, the shape of the phase diagram may depend on the electron and hole mass ratio, the anisotropy, the number of equivalent valleys in the valence and conduction bands, the frequency dependence of the dielectric constant, etc. A priori three qualitatively different situations are possible:

(1) The binding energy per electron–hole pair in the EHL $|E_1|$ exceeds $E_{ex}+\frac{1}{2}E_D$, the energy per single exciton in a molecule. In this case the EHL is energetically the lowest state of the non-equilibrium carrier system and at a sufficiently low temperature condensation occurs at any $n<n_1$. In this case the phase diagram has the qualitative appearance shown in figure 2(*a*).

(2) $E_1<E_{ex}+\frac{1}{2}E_D$. In this case the biexciton gas of low density ($n\to 0$), existing in a Bose-condensed state at low enough temperatures is the ground state of the nonequilibrium charge carrier system. However according to Brinkman and Rice [19] the effective interaction of biexcitons at low temperatures is strongly repulsive because of the absence of heavy particles and, consequently, the dominating role of quantum effects [19]. Thus with an increase in the level of excitation, the energy per excitonic molecule increases (decreases in absolute value) and at some $\bar{n}=n_{g0}$ becomes equal to $2E_1$; after that condensation occurs. The qualitative appearance of the phase diagram is illustrated in figure 4(*a*) for this case. Letters BG mark the area of gas degeneracy of the excitonic molecules. In the same way as the phase diagram in figure 2(*a*) was compared with the alkali-metal phase diagram, the phase diagram in figure 4(*a*) may be called hydrogen-like. However, the essential difference from the phase diagram of hydrogen is that the region in the hydrogen phase diagram corresponding to the classical molecular liquid and crystal corresponds to the quantum molecular gas region in figure 4.

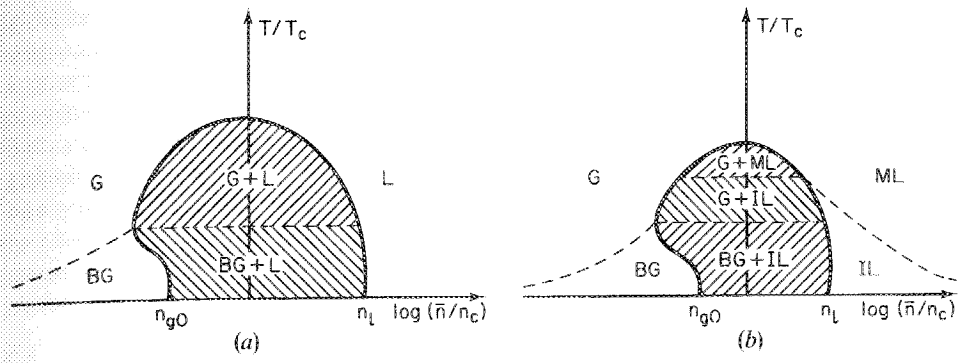

Figure 4. Phase diagram types, corresponding to a gas of Bose condensed excitonic molecules, BG being the ground state of the electron–hole system.

(3) So far the complete electron and hole delocalization in the EHL has been assumed to correspond to the usual metallic or, more exactly, semi-metallic nature of their energy spectrum. However, it is known [20–22] that in certain special cases, e.g. at single almost isotropic valleys for both electrons and holes, the semimetallic spectrum is unstable at low temperatures. Collective hole and electron interaction results in gap formation at the Fermi level and the spectrum becomes of insulator type. With increase in temperature or density the gap decreases and disappears; a semi-metallic state is restored. The phase diagram corresponding to this possibility is shown in figures 2(*b*) and 4(*b*), where the letters IL denote insulating liquid of the above type and ML a semi-metallic liquid. The region of separation into liquid and gaseous phases is hatched in figures 2 and 4. In different temperature intervals different phases coexist: one gaseous (G or BG) with one liquid (ML or IL). The B–BG and IL–ML transitions are likely to be second-order phase transitions and phase coexistence is impossible for them.

3.2.1. *Ground-state energy: dependence on band structure*

The question of which type of phase diagram corresponds to which type of semiconductor may be solved either by a quantitative theory, accounting for all the band structure peculiarities and other semiconductor parameters mentioned above, or experimentally. Quantitative theories of the EHL were initiated by Brinkman *et al.* [23], Combescot and Nozières [24], Brinkman and Rice [19], Vashishta *et al.* [25, 26]. The results of these and many other papers are described in reviews [7, 9]. Here I summarize only the most general results and then illustrate the EHL theory by a more complete examination of some simplified but correctly solvable models.

The most important factors for the determination of the type of phase diagram are the effective mass anisotropy and, especially, the multivalley structure of the electron and hole spectra. For the simplest case, when both the valence and conduction bands have one extremum with isotropic masses, all the existing calculations indicate $|E_1| < E_{ex} + \frac{1}{2}E_D$, i.e. in favour of one of the phase diagrams of figure 4. The largest calculated values for E_1 are $0{\cdot}99E_{ex}$ for the ML phase [25] and $1{\cdot}08E_{ex}$ for IL. The corresponding value of $n_1(T \to 0)$ is $0{\cdot}03a_{ex}^{-3}$ for the ML case. However, the energy difference $|E_1 - E_{ex} - \frac{1}{2}E_D|$ does not exceed a few per cent and, possibly, does not exceed the calculation accuracy. As explained above, the multivalley band structure essentially

enhances E_1 without noticeably changing E_{ex} and E_D. For semiconductors with an extremely anisotropic electron spectrum, particularly the so-called quasi-one-dimensional (polymer) and quasi-two-dimensional (layered) systems, or those with a large number of equivalent valleys, the problem of the EHL and its phase diagram turn out to be solvable exactly and analytically [27–29]. For such model system, as we shall now demonstrate, in agreement with the qualitative reasoning given above, the binding energy per particle pair in the EHL appears to be much greater than the exciton and excitonic molecule binding energies, and its equilibrium density is $n_1 \gg a_{ex}^{-3}$.

In the usual approach to the calculation of the ground-state energy of many interacting fermion systems this energy is expressed as a sum of three contributions

$$E(n) = E_0(n) + E_{exch}(n) + E_{corr}(n). \tag{7}$$

Here E_0 is the kinetic energy of the noninteracting particles, E_{exch} is the Hartree–Fock exchange energy and E_{corr} the correlation energy due to dynamic spatial correlation of the particles. The calculation of E_0 and E_{exch} is straightforward for any system and does not present any difficulties. It is the last term in (7) which depends on the complicated dynamics of the many-particle system and presents the main problem in the $E(n)$ calculation. In the case of the Coulomb interaction there exists a well-known general formula, expressing E_{corr} in terms of the polarizability of the system $\chi(\mathbf{k}, \omega)$, dependent on wave-vector $\mathbf{k}$ and frequency ω:

$$E_{corr}(n) = \frac{1}{2n} \int_0^1 \frac{d\lambda}{\lambda} \int \frac{d^3k d\omega}{(2\pi)^4} \left[\frac{4\pi\chi(\mathbf{k}, i\omega; \lambda)}{1 + 4\pi\chi(\mathbf{k}, i\omega; \lambda)} - 4\pi\chi^{(0)}(\mathbf{k}, i\omega; \lambda) \right]. \tag{8}$$

Here $\chi(\mathbf{k}, i\omega; \lambda)$ is the polarizability for an imaginary frequency $i\omega$, of the system of particles with charges $\pm\sqrt{\lambda}e$ (+ for holes) at concentration (density) n; $\chi^{(0)}$ is the first approximation of χ. In what follows it is natural to use 'excitonic' scales, i.e. to put $e^2/\varepsilon = \hbar = m = 1$. Then E is measured in units of E_{ex} and the only parameter in (8) is the dimensionless concentration n (na_{ex}^3). The only limiting case permitting a strict calculation of (8) is that of high density $n \gg 1$. In this case $\chi \approx \chi^{(0)}$ and higher-order corrections are of the order $p_F^{-1} \sim n^{-1/3} \ll 1$. This is the well-known random-phase approximation (RPA), described in any textbook on quantum many-body theory. Generally speaking, it is not appropriate for the EHL theory any more than for the theory of common metals, because the equilibrium densities corresponding to the minimum energy are of the order of unity. However, we shall now present a few model systems where the EHL equilibrium densities are $n_1 \gg 1$ and the RPA treatment appears to be adequate. The general feature of these models is that, owing to peculiarities of their band structure (multivalley, anisotropic), the Fermi momentum p_F and energy are anomalously small, and there exists a concentration range where

$$1 \ll p_F \ll n^{1/4} \tag{9}$$

holds. These model systems are:

(1) *Quasi-one-dimensional*, i.e. the system of conducting filaments with neglible transfer of electrons and holes from one filament to another and the density of filaments N (number per unit of surface area perpendicular to their direction) satisfies $Na_{ex}^2 \gg 1$ (i.e. $N \gg 1$ in dimensionless units). a_{ex} here is given by (4) with m the longitudinal mass. In this model p_F is determined by a linear concentration of carriers in every filament,

$$p_F = \frac{\pi}{2} \frac{n}{N}, \quad (N \ll n \ll N^{4/3}). \tag{10}$$

In the brackets here and below the range of concentrations satisfying inequalities (9) is indicated.

(2) *Quasi-two-dimensional*, i.e. a system of parallel conducting planes (layers) with interplane distance $c \ll 1$ (in units of a_{ex})

$$p_F = (2\pi nc)^{1/2}, \quad (c^{-1} \ll n \ll c^{-2}) \tag{11}$$

(3) *Multivalley or with large effective mass anisotropy*; if the number of valleys ν or the effective-mass ratio M/m can be considered as a large enough parameter for both electrons and holes, M and m—principle values of the mass tensor

$$p_{Fe,h} = \pi \left(\frac{3}{\pi} \frac{n}{\tilde{\nu}_{e,h}} \right)^{1/3}, \quad (\tilde{\nu}_{e,h} \ll n \ll \tilde{\nu}_{e,h}^{8/5}) \tag{12}$$

Here $\tilde{\nu} = \nu(M/m)^{1/2}$, if one of the effective masses M is much larger than the other two, and $\tilde{\nu} = \nu(M/m)$, if one of the effective masses m is much smaller than the other two. In both cases it is the smallest mass m which enters the exciton binding energy and the effective radius and, therefore, the definition of length and energy scales.

(4) *An electron–hole system in a strong magnetic field* $\mathscr{H} \gg 1$ (in units $\mathscr{H}_0 = e^3 m^2 c/\varepsilon^2 \hbar^3$). In this case, which is similar to the quasi-one-dimensional case, all the carriers are confined to the lowest Landau level and move freely in narrow 'Landau tubes' along the magnetic-field direction. The number of tubes per unit area of the plane orthogonal to the magnetic field is $\mathscr{H}/2\pi$:

$$p_F = 2\pi^2 \frac{n}{\mathscr{H}}, \quad (H \ll n \ll H^{4/3}). \tag{13}$$

In all these systems, owing to the respective large parameter $\Lambda = N, c^{-1}, \nu, M/m$ or $\mathscr{H}/2$, a concentration range exists which satisfies the inequalities (9) (as indicated in formulae (10)–(13) in brackets).

In this range, owing to the first inequality (9), the RPA is valid and, therefore

$$\chi(\mathbf{k}, i\omega; \lambda) \approx \chi^{(0)}(\mathbf{k}, i\omega; \lambda) = \frac{\lambda}{4\pi} V_{\mathbf{k}} \sum_{i=e,h} 2\Lambda_i \int \frac{d^d p}{(2\pi)^d} f_i(\mathbf{p}) \frac{\varepsilon_i(\mathbf{p}+\mathbf{k}) - \varepsilon_i(\mathbf{p})}{[\varepsilon_i(\mathbf{p}+\mathbf{k}) - \varepsilon_i(\mathbf{p})]^2 + \omega^2}. \tag{14}$$

In (14) $f_{e,h}(\mathbf{p})$ are Fermi distribution functions of electrons and holes, and $\varepsilon_i(p)$ their dispersion laws; d is the dimensionality of the system under consideration, which is unity for the cases of filaments and the strong magnetic field, two for the layered system and three for the multivalley system. $V_{\mathbf{k}}$ is the matrix element of the bare Coulomb interaction, accounting generally for structural peculiarities of the system (electron and hole confinement to filaments, layers, 'Landau tubes', etc.). But for wave-vectors which are small compared to the inverse structural unit length ($N^{1/2}, \mathscr{H}^{1/2}, c^{-1}$), which are only essential for the following considerations, this matrix element is always nearly equal to the Coulomb interaction Fourier transform, i.e. $V_{\mathbf{k}} \approx 4\pi k^{-2}$. The dominating contribution to the integral over wave-vectors in (8), as one can easily check below, comes from $|\mathbf{k}| \sim n^{1/4}$ and $\omega \sim n^{1/2}$, which owing to the second inequality (9) are large compared to p_F and E_F respectively. Therefore, only the values of $\chi^{(0)}$ corresponding to such momenta are needed, and in (14) $|\mathbf{k}| \gg p_F \gtrsim |\mathbf{p}|$ and $\varepsilon_i(\mathbf{p}+\mathbf{k}) \approx \varepsilon_i(\mathbf{k}) \gg \varepsilon(\mathbf{p})$. Then formula (14) reduces to

$$\chi^{(0)}(\mathbf{k}, i\omega; \lambda) \approx 2\lambda \sum_{i=e,h} \Lambda_i \frac{\varepsilon_i(\mathbf{k})}{|\mathbf{k}|^2[\varepsilon_i^2(\mathbf{k}) + \omega^2]} \frac{n}{\Lambda_i} = 2\lambda n \sum_{i=e,h} \frac{\varepsilon_i(\mathbf{k})}{|\mathbf{k}|^2[\varepsilon_i^2(\mathbf{k}) + \omega^2]}. \tag{15}$$

It should be remembered that $\varepsilon_i(\mathbf{k})$ (but not $|\mathbf{k}|^2$) depend here only on the d components of the wave-vector $\mathbf{k}$. In the multivalley case contributions to (15) of both electrons and holes should be averaged over all equivalent valleys, which may be differently oriented in momentum space. After substitution of (15) into (8) and the introduction of new integration variables $\mathbf{k}=(64\pi\lambda n)^{1/4}\ \xi$ and $\omega=(4\pi\lambda n)^{1/2}\zeta$,

$$E_{\mathrm{corr}}(n)=\frac{8}{5\pi^3}(4\pi n)^{1/4}\int \mathrm{d}^d\xi\,\mathrm{d}\zeta\, f(\xi,\zeta).$$

Here $f(\xi,\zeta)$ is a rational function depending on no other parameters than m_e/m_h. The evaluation of $E_{\mathrm{corr}}(n)$ now becomes straightforward and results in

$$E_{\mathrm{corr}}(n)=-\frac{32\pi}{5[\Gamma(\frac{1}{4})]^2}A_d\left(\frac{4}{\pi}n\right)^{1/4}\approx -1{\cdot}625A_d n^{1/4}. \tag{16}$$

The constant A_d depends on the dimensionality d of the system and very slowly on the electron and hole effective-mass ratio, but does not depend on the concentration n or the parameter Λ. In the case $m_e=m_h$, $A_3=1$, $A_2\approx 1,2$ and $A_1=2$.

The most remarkable features of (16) are universal for all models, that is, the dependence of E_{corr} on concentration as $n^{1/4}$ and its independence of Λ, whereas the values of $E_0(n)$ and $E_{\mathrm{exch}}(n)$ are strongly reduced in these models, owing to the large values of Λ.

The exchange energy in all these models appears to be small compared to the correlation energy, because, like $E_0(n)$, it is determined only by the concentration in one filament, layer, valley, etc. Therefore, (7) transforms to

$$E(n)=E_0(n)-An^{1/4}, \tag{17}$$

where $A\approx 1{\cdot}625\,A_d$. It is easy to check that for all cases under investigation $E(n)$ reaches its minimum in the concentration interval where inequalities (9) are valid. Let us demonstrate this claim for a quasi-two-dimensional system, where $E_0(n)=\frac{1}{2}\pi nc$. Then $A\approx 1{\cdot}95$,

$$n_{\min}\equiv n_1(T=0)=\left(\frac{A}{2\pi c}\right)^{4/3}\approx 0{\cdot}21c^{-4/3}, \tag{18}$$

$$E_{\min}\equiv E_1(T=0)=-\frac{3\pi}{2}\left(\frac{A}{2\pi}\right)^{4/3}c^{-1/3}\approx -0{\cdot}99c^{-1/3}. \tag{19}$$

Numerical results here and below correspond to the case $m_e=m_h$. Thus both the equilibrium concentration n_1 and the binding energy of the EHL are large (in units of a_{ex}^{-3} and $2E_{ex}$ respectively) if c is small enough compared to a_{ex}. From (18) $p_L\sim c^{-1.6}$ at the equilibrium density and both inequalities (9) are satisfied.

Not only the ground-state energy and the equilibrium density at zero temperature, but the whole thermodynamics of the EHL can be calculated for these models in the same way. For all temperatures $T\lesssim T_c$ the correlational contribution to the thermodynamic potential is the same as that given by (16), because the corresponding general formula differs from (8) only by changing the integration over ω to a sum over $\omega_j=2\pi jT$. But, as was seen, the principal contribution to this integral comes from $\omega\sim n^{1/2}\gg n^{1/4}\sim E_1\gtrsim T_c$. So for nonzero temperatures $E_0(n)$ in (17) has only to be replaced by the chemical potential of the noninteracting Fermi gas $\mu_0(n,T)$ in order to obtain the equation of state of the electron–hole system: $\mu(n,T)=\mu_0(n,T)-\frac{5}{4}An^{1/4}$.

Here $\mu(n, T)$ is the chemical potential of an electron–hole pair. For a quasi-two-dimensional system this looks like

$$\mu(n, T) = 2T \ln\left(\exp\left[\frac{\pi nc}{2T}\right] - 1\right) - \tfrac{5}{4}An^{1/4}. \tag{20}$$

The dependence (20) of μ on n at different temperatures is shown schematically in figure 5. The family of curves $\mu(n, T)$ has a typical van der Waals appearance and describes the coexistence of two phases. All the parameters of the phase diagram can be found from (20), including the equilibrium concentrations of both phases $n_l(T)$ and $n_g(T)$. The critical point is $n_c \approx 0{\cdot}036c^{-4/3} \approx 0{\cdot}17n_l(T=0)$, $T_c \approx 0{\cdot}102c^{-1/3} \approx 0{\cdot}103E_l(T=0)$. Note the excellent agreement with the empirical rule $kT_c \approx 0{\cdot}1E_b$, mentioned above. Three more qualitative results obtained from the analysis of equation (20) are worthy of special notice. The critical temperature appears to be very close to the Fermi degeneracy temperature, corresponding to $n = n_c$. This means that the electron–hole liquid actually exists only as a degenerate Fermi liquid. In the vicinity of the critical point the gas phase is a completely ionized electron–hole plasma and the transition is a gas–liquid type transition from a nondegenerate to a degenerate plasma. And, finally, within the model under consideration no other phase transitions occur except that of gas–liquid type with EHL formation.

Results for other models are similar and I will mention only the case of the strong magnetic field. In this case E_1 and T_c increase $\sim \mathscr{H}^{2/7}$, and n_1 and $n_c \sim \mathscr{H}^{8/7}$: $E_1(T=0) \approx -0{\cdot}42\mathscr{H}^{2/7}$, $n_1 \approx 0{\cdot}03\mathscr{H}^{8/7}$, or $E_1 \sim H^{2/5}$, $n_1 \sim \mathscr{H}^{6/5}$, if $m_h \gg m_e$ and electrons only are in the ultraquantum limit. As is known, the binding energy of the exciton increases in this limit as $\ln^2 \mathscr{H}$, and therefore, in a strong enough field the EHL becomes energetically favourable for arbitrary band structures. The most interesting property of

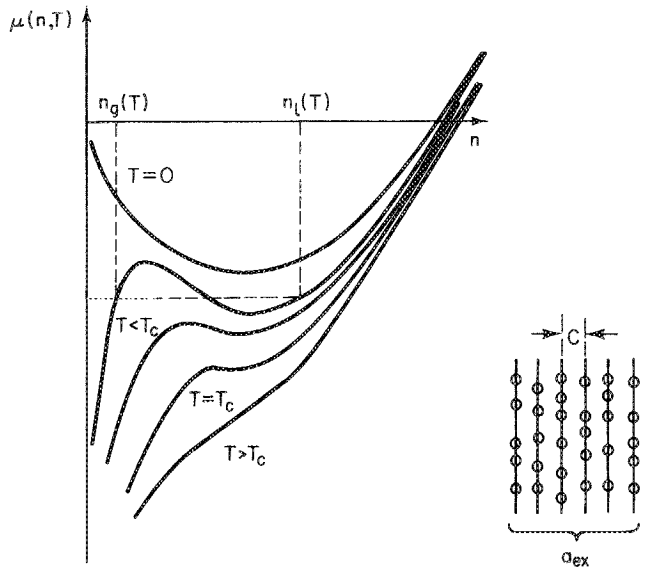

Figure 5. Equation of state of quasi-two-dimensional EHL in the μ–n plane (chemical potential–concentration plane) according to equation (20).

the EHL in a strong magnetic field is that it is insulating at low temperatures, as, owing to the one-dimensional character of the carrier movement, the appearance of the gap at the Fermi level becomes inevitable [30, 31]. This gap suppresses the scattering of carriers by phonons and thus greatly increases the EHL mobility. The coherent nature of the gap gives one reason to expect properties similar to superfluidity. The EHL is the only condensed matter which can be studied experimentally (in laboratories) in strong fields, corresponding to the ultraquantum limit. For usual matter the critical field for this regime is of the order 10^{10} G (10^6 T) and is inaccessible on Earth. However, such high fields are postulated under some astrophysical conditions (neutron stars, etc.).

Thus for semiconductors with multivalley band structure or sufficiently pronounced effective mass anisotropy the phase diagram of the nonequilibrium carrier system is certainly of the simplest shape, as depicted in figure 2(*a*). It is only in the case of single valley and not too anisotropic spectra of electrons and holes that the phase diagram of figures 4(*a*) and (*b*) might be realized: 4(*b*) for almost isotropic and not very different electron and hole masses and 4(*a*) for extremely different, moderately anisotropic masses. It should be emphasized once again that the accuracy of the existing calculations for single-valley, weakly anisotropic spectra does not enable us to eliminate completely the possibility that the phase diagram type of figure 2 is perfectly general.

The gas–liquid transition in the nonequilibrium carrier system is closely connected with the metal–insulator transition: from a weakly ionized poorly conducting exciton gas to a metallic EHL. The problem of the coexistence of these two transitions was first discussed (for mercury vapour condensation) in the well-known paper by Landau and Zel'dovitch [32]. The phase diagrams of figures 3 and 4 illustrate two different possibilities: complete coincidence of these transitions (figures 2(*a*) and 4(*a*)) and the case where the metal–insulator transition in some temperature interval occurs in the phase which is already condensed (figures 2(*b*) and 4(*b*)). Many authors (Insepov and Norman [33], Rice [7, 34], Ebeling *et al.* [35]) proposed still another possibility: that the metal–insulator transition should still occur in the gaseous phase owing to the screening of the Coulomb interaction, resulting in exciton destruction (the so-called Mott transition). However, well-known qualitative reasoning (Mott) [36] as well as the subsequent calculations show the Mott transition to be that of the first order and, consequently, to be accompanied by a specific volume change and a phase separation. Thus the dense phase formed in this transition possesses all the typical features of the EHL and there is no reason for the occurrence of still another phase transition at a further density increase.

3.2.2. *The influence of crystal ionicity*

Not only may the structure of the electron spectrum be different in different semiconductors, but also the nature of the electron–hole interaction may also be different. All the preceding considerations, as well as the theoretical papers mentioned above, are based on the assumption that the interaction is purely Coulombic and its specific character in a particular crystal is determined by only one constant—the dielectric constant. This assumption is well established for covalent semiconductors such as germanium and silicon. However, compounds such as gallium arsenide or cadmium sulphide are partially ionic and a noticeable contribution to their polarizability is due to the ion displacement, i.e. their lattice deformation. In such semiconductors the inertia of the heavy ions results in the Coulomb interaction becoming

retarded in time intervals of the order of the period of the lattice vibrations or, in other words, the dielectric constant becomes frequency dependent in the optical-phonon frequency region. In the random phase approximation (RPA) the introduction of the interaction with optical phonons into the calculation of the EHL energy corresponds [37] to the replacement of ε in (1) by the frequency-dependent dielectric constant $\varepsilon(\omega)$,

$$\varepsilon(\omega) = \varepsilon_\infty \varepsilon_0 \frac{\omega_1^2 - \omega^2}{\varepsilon_\infty \omega_1^2 - \varepsilon_0 \omega^2}. \tag{21}$$

Here ε_0 and ε_∞ are the static and high-frequency (electronic) values of the dielectric constant; ω_1 is the frequency of the longitudinal optical phonon. Such interaction naturally changes the exciton, biexciton and EHL binding energies and their ratios.

Direct calculations [7, 38–40] using (21) show that, in many polar semiconductors even with a small degree of crystal ionicity, the EHL becomes energetically more favourable than the biexcitonic gas, even with a single-valley spectrum and complete effective mass isotropy.

Finally let us make one more remark concerning the general status of EHL theory. The absence of heavy particles of nuclear type and the crystallization connected with them, the possibility of changing all the main parameters within a wide range, the comparatively easy accessibility of the so-called extreme conditions ($\bar{n} \sim n_c$, $T \sim T_c$ or $n \gg n_1$, superstrong magnetic fields), the possibility of observing directly binding energy and particle energy distribution in recombination radiation spectra, all these properties make the EHL an ideal model for the experimental and theoretical study of the quantum electron liquid—one of the fundamental objects of condensed-matter physics. Therefore, it is no wonder that practically all the methods invented for a theoretical description of the electron liquid in metals have also been tested in the EHL computations. As a matter of fact, all these methods are one or other modification of the RPA. Their general aim is to supplement the RPA treatment, which is asymptotically exact at very high densities $na_0^3 \gg 1$ (a_0 is the Bohr radius), in order to obtain a reasonable description at electron densities $na_0^3 \sim 10^{-1}$–10^{-3}, usual for metals. Taking into account certain factors (usually short-range electron–electron and electron–hole correlations, i.e. local-field corrections) and ignoring others, they are semi-empirical in the sense that there is no rigorous proof of the approximations used and no estimates of their accuracy within the theory itself for the density interval mentioned above. It is only the agreement with experiment that enables us to evaluate their real effectiveness. The same problem confronts EHL theory by changing only the scales of length a_0 and Rydberg by a_{ex} and E_{ex}. From this standpoint the success of the theory in application to the EHL would demonstrate the adequacy of the quantum many-body theory methods referred to above for the treatment of multielectron systems with densities typical for atoms, molecules and condensed media. However, the excellent agreement between the EHL theory and experimental data in Ge and Si described below should not be overestimated. Owing to the multivalley band structure and the strong effective mass anisotropy, the EHL equilibrium density in these semiconductors is abnormally great and really close to the limit of applicability of RPA. From this point of view, the absence of quantitative agreement between theory and experimental data in semiconductors with a simpler electronic spectrum might not be accidental, but may reflect the real limitations of the methods used in the domain of the usual 'metallic' densities $na_0^3 \sim 10^{-3}$–10^{-1}. Further experimental data on the EHL in different semiconductors and its systematic analysis will provide a final evaluation of these methods and probably indicate how to perfect them.

2.3. *Some experimental results*

Many excellent experimental studies of the EHL in semiconductors have been performed during the last fifteen years and are reviewed in [8, 9]. Only very few of them will be presented here in order to illustrate the most general and important EHL manifestations.

EHL experimental studies were started by Pokrovski and Svistunova [41] in 1969. In the spectrum of low-temperature luminescence of germanium they found the radiation due to the recombination of electron–hole pairs in the EHL.

The appearance of this radiation had a threshold character at decreasing temperature or increasing excitation level in accordance with the phase transition picture; its spectrum reflected the Fermi distribution of recombining carrier energies. Hence the equilibrium concentration in the EHL in germanium was determined to be $n_1 \approx 2 \times 10^{23}\,\mathrm{m}^{-3}$. Figure 6 [42] shows the luminescence spectrum of Ge consisting of the luminescence line of the free excitons (FE) and the recombination radiation line of the EHL for a very special choice of temperature at which the intensities of both lines are comparable. At the same excitation level but at a few tenths of a degree higher in temperature the EHL line completely disappears, but at a few tenths of a degree lower in temperature it becomes dominating and the exciton line decreases sharply. The line shape of the EHL luminescence corresponds to the calculated recombination radiation of a degenerate electron–hole plasma (solid line). Its full width equals the sum of electron and hole Fermi energies, and therefore only slightly depends on temperature; it is much larger than the line width of exciton luminescence, which is $k_B T$. The energy difference between the long-wavelength edge of the FE line and the short-wavelength edge of the EHL line is just the work function $\phi = |E_1 - E_{ex}|$ of the EHL. Thus luminescence data contain information concerning the main EHL parameters n_1, E_1 and also the electron and hole energy distribution in the EHL, n_g, and so on. Their study at different temperatures makes possible the reconstruction of the whole phase diagram of the nonequilibrium charge carrier system, as was done first for germanium [43] and silicon [44]. Up to now luminescence spectra have been the main source of information about the EHL and the only source for many direct-gap semiconductors with short lifetimes of non-equilibrium charge carriers.

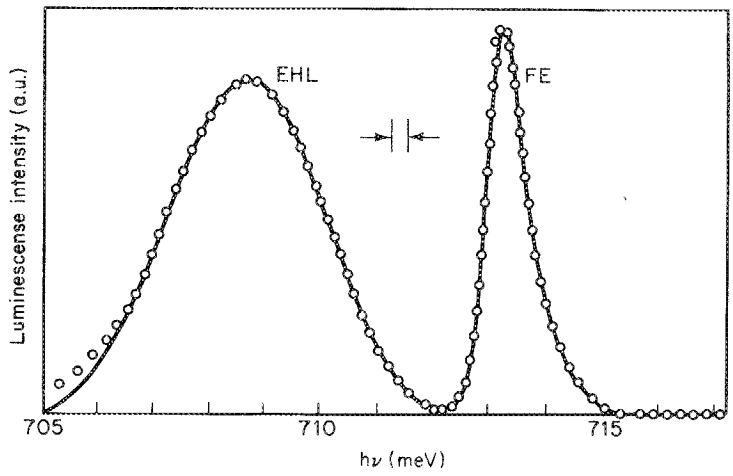

Figure 6. Low-temperature (3·5 K) luminescence spectrum of germanium, exhibiting free exciton (FE) and electron–hole liquid (EHL) recombination radiation lines [42]. The spectral resolution is indicated by the arrows.

in semiconductors have been
ed in [8, 9]. Only very few of them
ost general and important EHL

vski and Svistunova [41] in 1969.
of germanium they found the
e pairs in the EHL.
eshold character at decreasing
dance with the phase transition
of recombining carrier energies.
germanium was determined to be
nce spectrum of Ge consisting of
e recombination radiation line of
which the intensities of both lines
a few tenths of a degree higher in
t at a few tenths of a degree lower
n line decreases sharply. The line
iculated recombination radiation
Its full width equals the sum of
lightly depends on temperature; it
scence, which is $k_B T$. The energy
FE line and the short-wavelength
$\phi = |E_1 - E_{ex}|$ of the EHL. Thus
the main EHL parameters n_l, E_l
in the EHL, n_g, and so on. Their
econstruction of the whole phase
, as was done first for germanium
tra have been the main source of
many direct-gap semiconductors
iers.

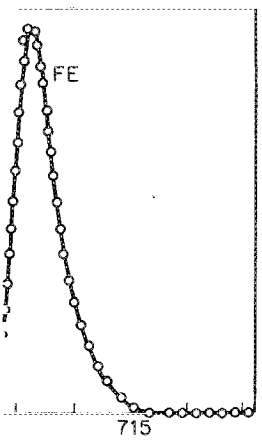

rum of germanium, exhibiting free
mbination radiation lines [42]. The

The phase diagrams of nonequilibrium charge carrier systems that have been most completely studied are in silicon and, more especially, germanium. The former is presented in figure 7. Both of them are undoubtedly of the simplest type of figure 2(*a*) owing to the multivalley band structure and the large effective mass anisotropy in both germanium and silicon. In both cases very good quantitative agreement of theoretically calculated values and experimental data (2–4% difference) is now achieved:

$$E_l(T=0) = 6\,\text{meV},\ n_l(T=0) = 2{\cdot}3 \times 10^{23}\,\text{m}^{-3},\ T_c = 6{\cdot}7\,\text{K},\ n_c = 0{\cdot}6 \times 10^{23}\,\text{m}^{-3}$$

in germanium and

$$E_l(T=0) = 23\,\text{meV},\ n_l(T=0) = 3{\cdot}5 \times 10^{24}\,\text{m}^{-3},\ T_c = 28\,\text{K},\ n_c = 1{\cdot}2 \times 10^{24}\,\text{m}^{-3}$$

in silicon. Note again the very accurate fulfilment of the rule $k_B T_c \approx 0{\cdot}1 E_l(T=0)$. In addition, another relation of the same type, namely $n_c = \text{const}\, n_l(T=0)$ has been proposed empirically [8] and theoretically justified by Vashishta *et al.* in [9] with const $\approx 0{\cdot}2$, but its accuracy is much poorer.

E_l values in germanium and silicon are relatively large, approximately 1·5 E_{ex}. There exists direct experimental evidence that this is due primarily to the multivalley band structure: the uniaxial stress of crystals, reducing the crystal symmetry and, therefore, the number of equivalent valleys, significantly reduces the EHL binding energy, critical temperature and equilibrium density [17]. In figure 8 the dependence of the energy maxima of free excitons and the EHL luminescence lines on the uniaxial stress P is depicted. The shift of the exciton position is approximately linear and follows that of the band gap E_g. But the EHL lines at small stresses shift in the opposite direction so that their distance from the exciton line, reflecting the EHL binding energy, decreases. And only for $P > P_{cr} \approx 2{\cdot}7 \times 10^6\,\text{kg m}^{-2}$, when all the electrons occupy only the two lower valleys instead of four in unstressed germanium (these two remain equivalent for this stress direction) the further shift of the EHL line becomes the same as that of the exciton line, i.e. the EHL binding energy becomes constant but smaller than

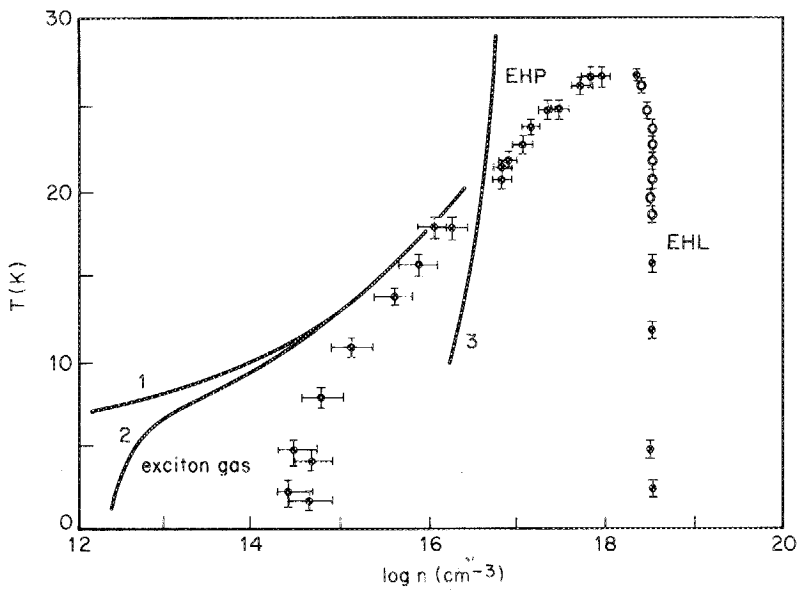

Figure 7. Phase diagram of nonequilibrium charge carrier system in silicon [44]. EHP nondegenerate electron–hole plasma, 3 theoretical Mott transition curve.

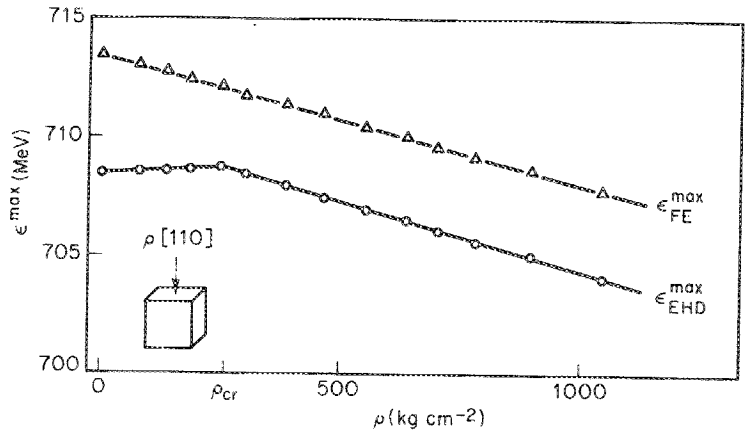

Figure 8. Stress dependence of positions of the maxima of FE and EHL lines, shown in figure 6 for $T=3$ K [17].

at zero stress. The same experiments [17] demonstrated that non-uniformity of the stress results in the fast movement of EHDs in the direction of increasing stress. At moderate stresses $P \gtrsim P_{cr}$ they travel for a distance of the order of 1 cm with velocities close to that of sound. This phenomenon provided makes possible the aggregation of a cloud of small EHDs into one 'large drop' [45]—a macroscopic volume of the EHL, which is very convenient for the investigation of the properties and the many new fascinating phenomena in the EHL, including its direct visualization, as described by Wolfe and Jeffries [9].

There exist many manifestations of two-phase coexistence in the non-equilibrium carrier system at $T<T_c$. One of the most spectacular is the time dependence of the exciton concentration in the gas phase n_g after excitation of a specimen by a short intense illumination pulse at $t=0$ (figure 9) [46]. It differs drastically from the usual exponential decay with lifetimes of 4–8 μs which one observes in this type of experiment but at higher temperatures or lower excitation levels. Instead, the concentration of

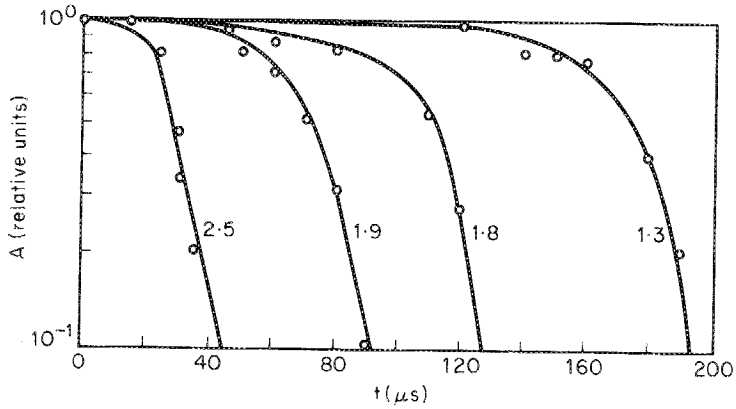

Figure 9. Time decay of exciton concentration under the conditions of existence of EHL in a germanium sample, excited by an intense short pulse at $t=0$ [46]. The values 2·5, 1·9, 1·8 and 1·3 show preliminary attenuation of the exciting pulse compared to some maximum value.

excitons coexisting with the EHL remains virtually constant during time intervals exceeding 20–30 times their lifetime, because evaporation of new excitons from the EHDs just compensates their recombination in the gas phase, maintaining the equilibrium value $n_g \approx n_s(T)$ (saturated vapour pressure). And only after the disappearance of all EHDs due to recombination and evaporation, does the remaining exciton concentration decrease fast with the usual lifetime. Obviously, the time interval of constant (quasi-equilibrium) exciton concentration increases as the initial total volume of the EHL increases. This also agrees with the data given in figure 9, where the numbers on different curves designate the attenuation of the preliminary exciting-pulse relative to some maximum value.

The Fermi liquid nature of the EHL was first demonstrated by the observation of the oscillatory dependence of its luminescence intensity on magnetic field [47]. This dependence is shown in figure 10 together with the Landau levels of electrons and holes, as a function of the magnetic-field strength $\mathscr{H}$, and the crossing of these levels with the Fermi levels E_{Fe} and E_{Fh}. The reason for these oscillations is the same as for the de Haas–van Alphen effect. Like any other thermodynamic quantity, the equilibrium concentration of the EHL oscillates as a function of the quantizing magnetic field, and, therefore, the probability of radiative recombination also oscillates [48]. At still larger fields all electrons are in the lowest Landau level, i.e. the ultraquantum limit is reached.

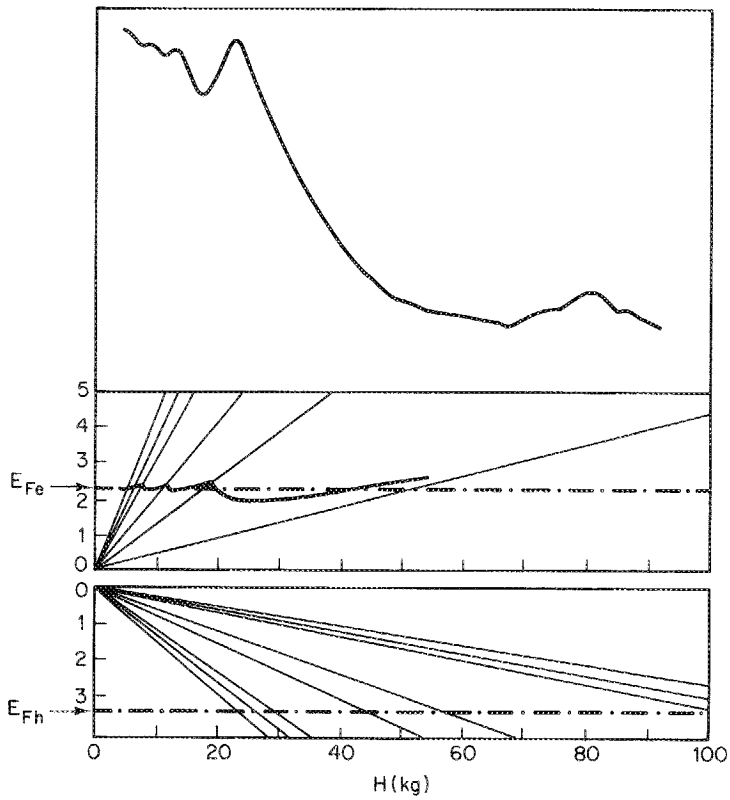

Figure 10. Magnetic-field dependence of the intensity of EHL luminescence in germanium, $H \| [100]$, $T = 1{\cdot}5$ K. Also shown are Landau levels in conduction and valence bands, crossing electron and hole Fermi levels [47].

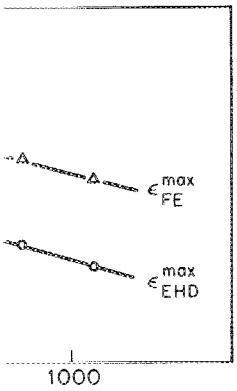

FE and EHL lines, shown in figure 6

ated that non-uniformity of the
direction of increasing stress. At
the order of 1 cm with velocities
ikes possible the aggregation of a
nacroscopic volume of the EHL,
e properties and the many new
ect visualization, as described by

existence in the non-equilibrium
ar is the time dependence of the
tation of a specimen by a short
differs drastically from the usual
bserves in this type of experiment
ls. Instead, the concentration of

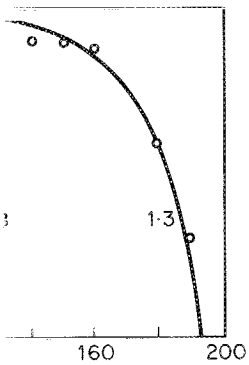

conditions of existence of EHL in a
e at $t = 0$ [46]. The values 2·5, 1·9, 1·8
g pulse compared to some maximum

An approximately linear increase of the equilibrium EHL density with magnetic field strength was reported in this regime [49], closely corresponding to the above theoretical prediction. But any experimental evidence for the existence of the insulating liquid phase is still lacking, and it remains one of the most intriguing possibilities of future EHL research.

Other manifestations of the Fermi liquid state of the EHL are the observation of plasma resonance [50], Alven waves [51] and the direct measurement of conductivity [52], which appeared to be rather large, corresponding to a carrier momentum relaxation time 10^{-10}–10^{-11} s, limited probably be electron–hole scattering. It should be noted that the relaxation time of the momentum of the EHD as a whole, measured in experiments with EHD movement, appears to be two orders of magnitude larger, because obviously interparticle collisions inside the EHD do not contribute to this relaxation, and it is determined only by electron–phonon scattering. All the data described above, like many other, refer to germanium and silicon.

There are numerous reports on the observation of the EHL and the establishment of its phase diagram in many other semiconductors, most of them reviewed by Kulakovskii and Timofeev in [9]. However, as a rule, these data are less complete and conclusive as compared with those on germanium and silicon and obtained only from spontaneous- or stimulated-luminescence data. In connection with the above discussion of possible types of phase diagram, special interest attaches to materials with one valley and a more or less isotropic spectrum, such as gallium arsenide or cadmium sulphide. Though it is too early to draw any final conclusions, it seems that, in spite of the above-mentioned theoretical estimates, experimental data on these semiconductors give evidence in favour of a phase diagram of the type of figure 2 (*a*). The cause of this discrepancy (perhaps not the only one) may be that all these semiconductors are partially ionic, which, as explained above, changes the stability conditions of the EHL. Accounting for the frequency dependence of the dielectric constant in some cases eliminates the qualitative contradiction of theory and experiment concerning the type of phase diagram, but fails to produce quantitative agreement similar to that achieved for germanium and silicon: calculated values of the EHL binding energy remain smaller and equilibrium densities essentially larger than those reported in experimental studies. Also the results of calculations by different authors are noticeably different. Perhaps the reason is the inadequacy of the RPA and other methods closely related to it because of the relatively small ($\sim 10^{-2}$) equilibrium density in the single-valley semiconductors.

4. Electron–hole drops

4.1. *Kinetics of electron–hole drop nucleation, growth and decay*

The concepts of phase diagram, phase transition, phase coexistence, etc., strictly speaking, refer to systems in thermodynamic equilibrium. For a description of the nonequilibrium charge carrier system in semiconductors they are applicable only approximately, according to the smallness of the thermalization time, i.e. the relaxation time of the carrier kinetic energy, compared with their lifetime, determined by recombination processes. This time ratio reaches 10^4–10^5 in the case of Ge and Si and 10–10^2 in the so-called direct-band semiconductors of groups $A^{III}B^{V}$ and $A^{II}B^{VI}$, of which gallium arsenide and cadmium sulphide are typical examples. Thus with a greater or lesser degree of accuracy thermalization occurs if the lattice temperature is not too low. But even if carrier thermalization may be considered complete, the finite carrier lifetime qualitatively changes some details of the phase diagram and produces

quite a number of phenomena and properties that distinguish the EHL from any other liquid. The reason is that the condensation process itself, i.e. the formation of liquid-phase nuclei and their further growth to the macroscopic EHD, is much slower than thermalization, as it requires the participation of a macroscopically large number of particles. At this stage the finite carrier lifetime plays a decisive role. It limits the EHD growth, complicates the nucleation process, etc. However, it does not limit the existence time of the EHD if some excitation source continuously produces new electron–hole pairs whose condensation compensates the recombination in the EHL volume.

From this point of view, all experiments with the EHL can be divided into two essentially different groups: stationary and pulsed. In the latter the specimen is excited by a short intense pulse with duration less than the carrier lifetime, and subsequent EHD formation and decay are observed. The growth (or decay) kinetics for every individual EHD is described by a simple balance equation [3, 53] for the total number of particles in it:

$$\frac{\mathrm{d}}{\mathrm{d}t}\left(\frac{4\pi}{3}R^3 n_1\right)=4\pi R^2\gamma v_T[n-n_g(T,R)]-\frac{4\pi}{3\tau_1}R^3 n_1, \tag{22}$$

where R is the spherical EHD radius, n is the exciton concentration in the gaseous phase, v_T is their thermal velocity, γ the so-called accommodation coefficient, i.e. the probability of an exciton approaching the EHD being absorbed, τ_1 and n_1 the carrier lifetime and their equilibrium concentration in the EHL. The first term on the right-hand side is the difference between the number of excitons captured by the EHD surface from the surrounding gas and the number evaporated from this surface. The flow of evaporated excitons from the detailed-balance condition is expressed in terms of the gas concentration $n_g(T,R)=n_g(T)\exp[2\sigma/n_1 RT]$ (σ is the EHL surface tension), which would be in equilibrium with EHD of radius R at a given temperature in the absence of recombination. The second term on the right-hand side of equation (22) is the recombination rate in the EHD volume. A complete quantitative description of the condensation kinetics in the nonequilibrium charge carrier system is based on the nucleation analysis and the time evolution of the EHD size distribution function [53–59]. But the qualitative picture of the phenomena and the significance of the recombination process in them can already be understood from equation (22).

Figure 11 presents schematically three curves corresponding to temperatures $T_1>T_2>T_3$ and describing the connection of $\Delta n=n-n_g(T)$ (gaseous-phase supersaturation) with the EHD radius R in a stationary state, obtained by equating the righthand side of equation (22) to zero. The domain of parameter values $(\Delta n, R)$ above such a curve corresponds at a given temperature to growing EHD, i.e. $\mathrm{d}R/\mathrm{d}t>0$, and the domain under this curve to decaying EHD, $\mathrm{d}R/\mathrm{d}t<0$. The typical U-shaped form of the curves for T_1 and T_2 is due to the combined action of two factors. At small R surface tension diminishes the work function of the droplet and in this way increases the pressure of the saturated vapour above it. At larger R the supersaturation, necessary to support the drop in a steady state, increases because the exciton flux must compensate for the recombination inside the drop, and this flux is proportional to supersaturation and surface area, while the number of recombining particles grows with the volume of the drop. The first of these effects is common to any liquid. The second is due to the finite lifetime of nonequilibrium carriers and is specific to the EHL. It produces in the curves $\Delta n(R,T)$ of figure 11 a characteristic minimum at $R=R_{\min}(T)$,

$$R_{\min}(T)=\frac{1}{n_1}\left[\frac{6\sigma\tau_1\gamma v_T n_g(T)}{k_B T}\right]^{1/2}. \tag{23}$$

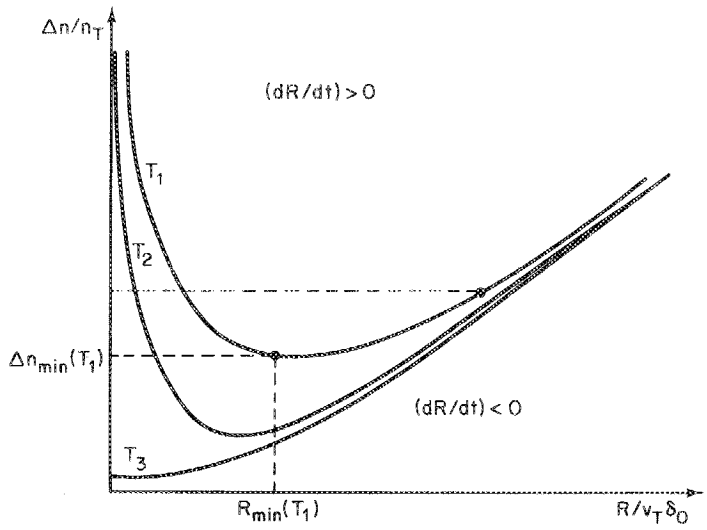

Figure 11. Super-saturation of the exciton gas against steady-state electron hole drop radius for different temperatures $T > T_2 > T_3$. At a temperature T, R_{min} (T) is the minimum stable EHD radius and $\Delta n_{min}(T)$ the minimum saturation necessary for EHD existence.

The supersaturation corresponding to this point,

$$\Delta n_{min}(T) = 2\left[n_g(T)\frac{2\sigma^*}{3v_T\gamma\tau_1 k_B T}\right]^{1/2}, \tag{24}$$

is at a given temperature the minimum supersaturation; only above this can the EHD exist. Therefore, because of kinetic factors, the threshold nonequilibrium carrier concentration for condensation is $n_g(T)+\Delta n_{min}(T)$, and not simply $n_g(T)$, determined from the thermodynamic equilibrium conditions of the EHL and the carrier and exciton gas.

There are two stationary values of R for every $\Delta n > \Delta n_{min}$. However, it is easy to understand that only one value of R, that on the ascending $(R > R_{min})$ branch of the curve $\Delta n(R)$, is stable, because the signs of dR/dt at the (n, R) plane sections close to this branch, are such that, even after an accidental small deviation of R from its stationary value at given Δn, R returns to its original value. By contrast the stationary values of R at the descending $(R < R_{min})$ branch are unstable: after a small deviation they do not return, but tend either to $R \to 0$ or to the ascending branch. They correspond to the so-called critical nuclei, well known in condensation theory. The average picture considered above does not enable us to describe their formation process, as according to (22) droplets with sizes less than that of a critical nucleus at given Δn do not grow, but evaporate. Critical nucleus formation requires a big fluctuation to overcome the thermodynamic barrier, separating the exciton gas (in figure 11 it corresponds conventionally to $R \to 0$) from the EHL, consisting of macroscopic EHD with radii on the ascending branch. The reverse process is also possible; then the barrier is overcome in the opposite direction from the liquid phase side: a fluctuational decrease of the stationary existing EHD to the critical embryo size with its subsequent evaporation. In a more elaborate description, accounting for fluctuations and EHD size distribution [54–59], stable R values correspond to sharp maxima of a distribution function and

critical embryo size to a deep minimum. The greater the embryo size and the smaller Δn, the less is the probability of a fluctuation necessary for this embryo formation. Therefore, when Δn rising reaches Δn_{min}, the EHD existence becomes possible; virtually, however, they do not appear as an enormous time is required for their nucleation. The gaseous phase remains metastable. Only at considerably larger Δn, corresponding to a smaller size of the critical embryo, does intense formation of EHD start. If Δn is then lowered again, all EHD diminish in size according to the $\Delta n(R)$ curve of figure 11 but continue to survive down to Δn values only slightly exceeding Δn_{min}, when the probability of their evaporation due to fluctuations already becomes overwhelming. Thus, at concentrations not greatly exceeding the condensation threshold value, the nonequilibrium carrier system possesses pronounced hysteresis [60], as the EHD number and the total volume of the liquid phase depend not only on the present excitation level, but also on its prehistory. This behaviour is typical of first-order phase transitions and is not in the least peculiar to the EHL. But the EHL is unique inasmuch as the memory of initial conditions is preserved in it during times many orders of magnitude greater than the lifetime of the electrons and holes of which it is composed [61, 62].

With a decrease in temperature the minimum value $R_{min}(T)$ of the stable radius of the EHD quickly diminishes and at sufficiently low temperatures becomes $\sim n_i^{-1/3}$. This means that droplets containing only a few pairs of particles are involved. Essentially these are not yet EHL droplets but the so-called multiexciton complexes. It is clear that continuing the curves in figure 11 into the range of still smaller R is meaningless. Therefore, at such and still lower temperatures the $\Delta n(R)$ dependence assumes the appearance depicted in figure 11 by the curve T_3 with no minimum and no descending branch corresponding to critical embryos. Therefore, there exists no thermodynamic barrier to EHD formation. And this changes the condensation picture drastically [54–59]. Hysteresis phenomena are completely absent. The system responds to an increase in excitation level, first of all by increasing the number of complexes being formed. The size of each of them remains very small and they grow only slowly with excitation level. Close to threshold these are complexes of a few excitons and it is only at essentially larger excitation levels that they acquire all the characteristic features of EHL drops, including definite and constant values of n_l and E_l. Just such a picture was observed at low temperatures in Si [63] and later in other semiconductors. Under such conditions nonequilibrium charge carrier condensation loses all the typical features of a first-order phase transition. A difference between the gaseous and the condensed phase gradually develops as the excitation level increases, corresponding rather to a second-order phase transition picture [64, 65]. Perhaps it would be more correct to speak of the absence of a well-defined phase transition, because the formation of the multiexciton complexes has no definite threshold. The process only weakly depends on the temperature and becomes noticeable at carrier concentrations determined by the competition between the elastic capture of excitons and their recombination.

Figure 12 shows schematically the EHD existence region under stationary excitation conditions, taking into account the above discussion on the role of the charge carrier finite lifetime and the absence of equilibrium associated with it. For comparison the branch $n_g(T)$ of the phase diagram of figure 2 (*a*) corresponding to the system in the thermodynamic equilibrium is also shown.

In the case of pulse excitation it is the mutual influence of EHL and exciton gas that most noticeably manifests itself. Generally the decay kinetics of both phases appear to

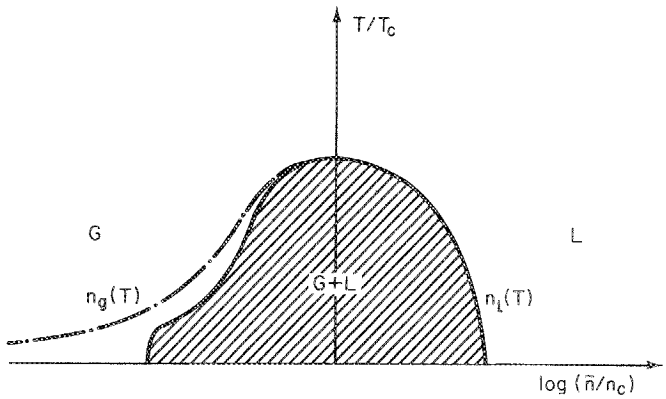

Figure 12. Electron–hole drop existence region accounting for the effect of charge carrier finite lifetime. The broken line is the $n_g(T)$ low-density branch of the phase separation curve of figure 2(*a*).

be essentially nonexponential. At sufficiently low temperatures EHD evaporation maintains the exciton concentration at a nearly constant level (saturated vapour pressure) for a time longer by more than an order of magnitude than the exciton lifetime and several times greater than the charge carrier lifetime in EHDs themselves, as shown in figure 9 and explained above. At higher temperatures it is evaporation and not recombination that is the dominant decay mechanism for sufficiently small droplets. In this case the reduction of the EHD radius occurs not exponentially with time but linearly [8]. EHDs completely disappear in a time interval which at small initial supersaturation may be considerably less than the carrier lifetime, recombination occurring mainly in the gaseous phase.

The most powerful method of direct observation and investigation of EHDs is that of light scattering [66–71]. In this type of experiment both the EHD radii and their number can be measured. In figures 13 and 14 the temperature dependences of these quantities are shown at a fixed excitation level. Typical values of EHD radii in germanium are 1–10 μm and increase as the temperature increases. The number of drops per unit volume N decreases rapidly at higher temperatures, typical values being 10^9–$10^{14}\,m^{-3}$. Both temperature dependences can be easily understood in terms of the above considerations. The number of drops is determined by the nucleation process which increases very rapidly with supersaturation. At a given excitation level immediately after the excitation source is switched on, nucleation still starts and the exciton concentration is the same for any temperature. This means that the relative supersaturation is much higher at low temperatures than at higher temperatures, because the threshold concentration decreases rapidly with temperature. Therefore, at low temperatures the nucleation process is very fast. While growing, these EHDs absorb excitons, supersaturation reduces and the birth of new nuclei stops. The total number of nonequilibrium charge carriers is fixed by the excitation source, and it relates the radii of the EHD with their number. So at low temperatures many small drops arise, and at higher temperatures a smaller number of larger drops. It is interesting that under stationary conditions all drops have the same radius, since it is

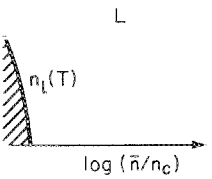

g for the effect of charge carrier finite
nch of the phase separation curve of

emperatures EHD evaporation
onstant level (saturated vapour
agnitude than the exciton lifetime
ne in EHDs themselves, as shown
atures it is evaporation and not
for sufficiently small droplets. In
not exponentially with time but
interval which at small initial
carrier lifetime, recombination

nd investigation of EHDs is that
it both the EHD radii and their
mperature dependences of these
ypical values of EHD radii in
rature increases. The number of
emperatures, typical values being
easily understood in terms of the
mined by the nucleation process
n. At a given excitation level
n, nucleation still starts and the
re. This means that the relative
es than at higher temperatures,
y with temperature. Therefore, at
st. While growing, these EHDs
th of new nuclei stops. The total
by the excitation source, and it
at low temperatures many small
number of larger drops. It is
have the same radius, since it is

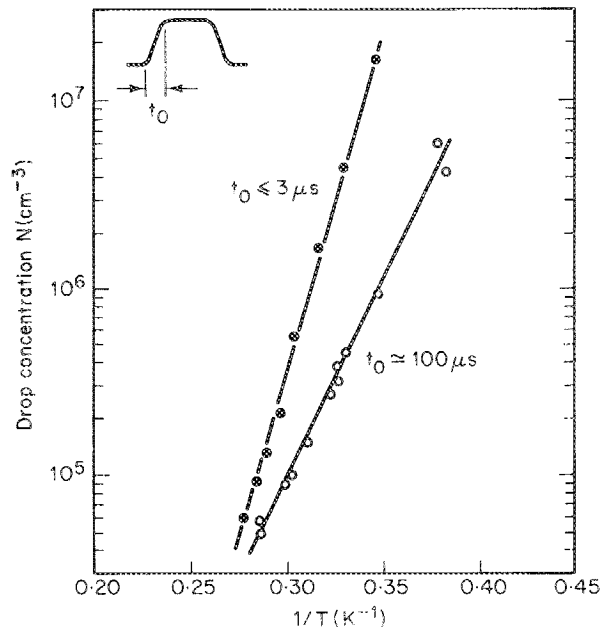

Figure 13. Temperature dependence of the number of electron–hole drops per unit volume. Different curves correspond to the same excitation levels, but with different rise times t_0 [70].

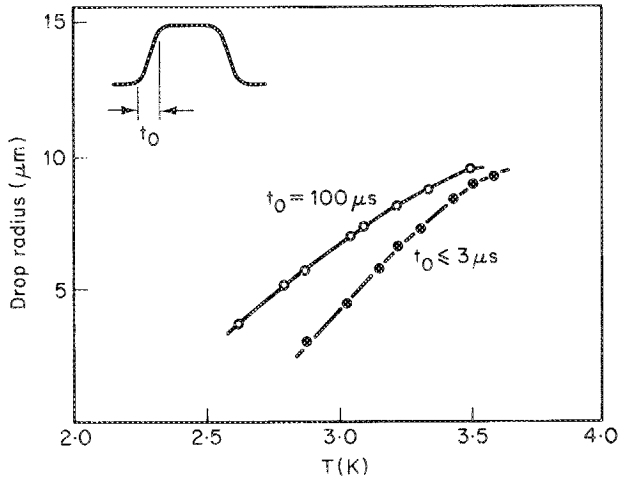

Figure 14. Electron–hole drop radii under the same experimental conditions as in figure 13 [70].

determined, as figure 11 shows, only by the exciton concentration in the gas phase. Strictly speaking, this claim refers only to drops in a volume whose linear dimensions do not exceed the exciton diffusion length, which is ~1 mm in germanium. Different curves in figures 13 and 14 correspond to different rise times of the same excitation level and thus demonstrate the dependence of the drop number on the initial supersaturation and the subsequent memory of this initial period of their formation.

Figure 14 shows also that, corresponding to different experimental conditions, both curves tend to saturation at the same limiting value $R = 10\,\mu$m. Indeed detailed investigation [70] shows that neither a further increase in excitation level nor in temperature results in EHD radii exceeding this value. Reaching it, all the curves become constant. The only exceptions are the 'large drops' artificially produced by a nonuniform strain of the crystals mentioned above. The reason for this sharp limitation on the EHD radii in unstrained crystals is explained below. The unusual quantum nature of the accommodation coefficient γ is also worthy of notice. There exists experimental evidence that γ is relatively small, $\sim 0{\cdot}1$, but increases with temperature. The probable reason seems to be the absence of heavy particles and the pronounced quantum effects for excitons. In some approximation the EHD may be treated as a potential well for excitons with a sharp boundary. The width of the boundary is $\sim n_1^{-1/3} \sim a_{ex}$, much smaller than the exciton de Broglie wavelength $\hbar(mk_BT)^{-1/2}$, if $k_BT \ll E_{ex}$. However, it is a well-known quantum-mechanical effect that the reflection coefficient for slow particles from a potential well tends to unity as the particle energy tends to zero. In other words, the probability of exciton penetration into the EHD tends to zero as $(k_BT/E_{ex})^{1/2}$. This effect is absent in ordinary gas–liquid systems, because owing to the presence of heavy nuclei the de Broglie wavelength of the atoms remains small in atomic units at all temperatures and the interface boundary cannot be treated as sharp.

4.2. *Moving drops*

One of the most remarkable features of EHDs is their high mobility. They can be accelerated by spatially nonuniform magnetic and electric fields, deformations, and so on. Among these possibilities nonuniform deformation is the most effective. As a matter of fact, the forbidden gap E_g, i.e. the electron–hole pair energy at rest, is known to depend on stress. Therefore, in nonuniformly strained crystals the energy of every electron–hole pair and of the EHD as a whole is different at different points, being equivalent to some potential energy. This means the existence of forces proportional to the local deformation,

$$\left.\begin{aligned} \mathbf{f} &= -n_1 \operatorname{grad}(D_{ik}\varepsilon_{ki}), \\ D_{ik} &= D_{ik}^{(e)} + D_{ik}^{(h)}. \end{aligned}\right\} \tag{25}$$

Here $\mathbf{f}$ is the volume force density, $D_{ik}^{(e,h)}$ the deformation potentials for electrons and holes, and ε_{ik} are the deformations. The movement of the drop is damped owing to the scattering of carriers by thermal phonons. But at low temperature the damping is reduced by the Fermi degeneracy of the carriers and decreases as T^5. At liquid helium temperature the value of the damping coefficient is of the order of $10^9\,s^{-1}$ in germanium. That means that at stresses of the order $10^7\,kg\,m^{-2}$ EHDs can be accelerated to a speed close to that of sound, as was experimentally demonstrated in [17]. Up to now there exists no experimental evidence of EHD movement with a velocity exceeding that of sound, perhaps because of additional damping or even the disintegration of the drop by coherent radiation of Mach waves. But even with smaller velocities they can travel during their lifetime macroscopic distances as large as 0·1–1 cm.

4.3. *The phonon wind*

At excitation levels reasonably exceeding the threshold value another set of phenomena related to the so-called 'phonon wind' becomes crucial for condensation kinetics

[72, 73]. The point is that most of the excitation energy eventually dissipates into heat, i.e. into phonons. Phonons are emitted both during the thermalization process of nonequilibrium carriers immediately after their creation and as a result of their subsequent recombination. Therefore, the areas where carrier generation takes place and EHDs exist and where excitation energy is concentrated are sources of strong nonequilibrium phonon fluxes. Interacting with carriers, free or bound in excitons, biexcitons and EHDs, phonons are partially reabsorbed and transfer their energy and momentum (or, more accurately, quasimomentum) to the carriers. The average momentum transferred to the carriers per time unit is equivalent to an effective force acting on the carriers. Its value is proportional to the phonon flux density, the direction being determined by that of their propagation. In a certain approximation EHL volume forces produced by the phonon wind are similar to the electrostatic forces in a uniformly charged liquid. In fact, every element of the EHL volume is a source of radially propagating phonon flux, whose density decreases in inverse proportion to the square of the distance. Consequently any two elements of the EHD, whether they are within the same EHD or belong to different EHDs, repel each other with a force inversely proportional to the square of the distance between them, i.e. as if in agreement with the Coulomb law. Thus the EHL may be characterized by some effective charge density ρ which has nothing to do with any real electric charge, but can be expressed in terms of the concentration of electron–hole pairs, their recombination rate, the emitted phonon spectrum, the effective cross-section of their absorption, etc.

$$\rho^2 = C\frac{n_1^{4/3}E_g}{\tau_1}\frac{D^2m^2}{\hbar^2 ds^2}. \tag{27}$$

Here D is the deformation potential, d the crystal density and s the sound velocity. Only long-wave phonons with momenta $|\mathbf{k}| \leqslant 2p_F$ interact with carriers. Therefore, the coefficient C accounts for the part of dissipated energy released in these phonons. Crude estimates give $C \sim 10^{-2}$, $\rho \sim 10^2$ CGSE in Ge and $\rho \sim 10^4$ CGSE in Si.

One of the most striking manifestations of the phonon wind is the instability of large EHL volumes [73]. The phonon wind strength grows in proportion to the EHD linear size and, as the droplet radius exceeds some critical value,

$$R_c = \left(\frac{15}{2\pi}\frac{\sigma}{\rho^2}\right)^{1/3} \tag{28}$$

(σ is the EHL surface tension), the force produced by the phonon wind exceeds that of the surface tension. The EHD becomes unstable to quadrupole deformation and divides into two drops with radii less than R_c, as shown in figure 15.

This process is quite similar to the fission of a large atomic nucleus. Thus the EHD cannot grow to sizes larger than R_c. This explains the limitation on the radii of EHDs discussed above and in figure 11 the curves must be limited both at small and large values of R: $n_1^{-1/3} \lesssim R \leqslant R_c$. According to theoretical estimates and some experimental data in germanium $R_c \simeq 10\,\mu$m and in silicon $R_c \sim 1\,\mu$m. This claim does not contradict the observation mentioned above of much larger drops in germanium [45], because these drops are strain confined. There exist experimental indications that in silicon such large drops do not exist, owing to the much more intense phonon wind. Instead, under the conditions of a strain-produced potential well, a cloud of small droplets arises, hanging in the field of the phonon wind produced by themselves [74]. The formation of an EHL volume with size considerably exceeding R_c is also possible as a result of a

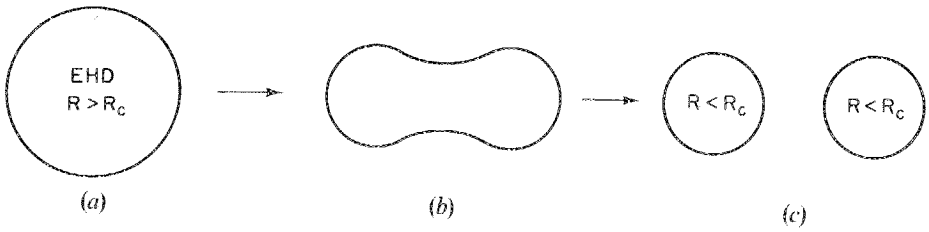

Figure 15. Deformation (*b*) and division (*c*) of electron–hole drops induced by phonon wind.

short intense exciting pulse, immediately producing an electron–hole pair concentration $n \geqslant n_1$ in a given volume. The subsequent events, shown in figure 16, remind one of a microexplosion. Under the action of the phonon wind the EHL surface becomes unstable: the so-called capillary wave amplitudes increase, so that EHDs with sizes of the order R_c begin to break off from it. This process continues until the whole EHL volume transforms into a cloud of EHDs, flying away due to mutual repulsion: the bigger the initial EHL volume, the greater the velocities of the drops. A similar flying-apart also occurs in the case on an exciting pulse producing not a single large EHL volume, but a dense cloud of small EHDs. This EHD cloud flying off in different directions at near-sonic velocities was observed experimentally for the first time by Damen and Worlock [71]. The dynamics of this process, shown in figure 17, has been well studied experimentally [75, 76]. It is extremely anisotropic owing to the anisotropy of the sound velocity and the deformation potential [77]. Impressive photographic images of the cloud of EHDs ejected from the excitation region under stationary and pulsed conditions are shown in figures 18 and 19 [77, 78]. The ejection of EHDs from the initial excitation region was shown to occur not only because of their mutual repulsion. It is clearly visible in figures 17 and 19 that the EHD clouds move away as a whole from the point where they were born. Evidently the phonon flux produced in the carrier thermalization process is of considerable importance. However, it is quite unexpected that this flux should exist after the end of the excitation pulse. During a time some orders greater than the carrier thermalization time the phonon wind source, the so-called 'hot spot', exists in the initial excitation region [79]. It is likely that the optical and short-wave acoustic phonons with a small free-path length, generated during the thermalization process, cannot leave the generation region, but

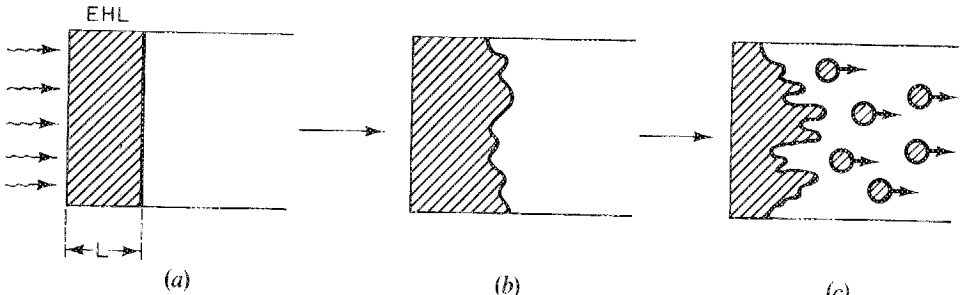

Figure 16. (*a*) Formation of a large EHL volume, (*b*) growing capillary wave instability of surface and (*c*) decay of an initial volume into a cloud of flying-away electron–hole drops.

(c)

ole drops induced by phonon wind.

ıg an electron–hole pair con-
ents, shown in figure 16, remind
phonon wind the EHL surface
ıdes increase, so that EHDs with
rocess continues until the whole
; away due to mutual repulsion:
elocities of the drops. A similar
lse producing not a single large
EHD cloud flying off in different
rimentally for the first time by
ess, shown in figure 17, has been
ely anisotropic owing to the
tion potential [77]. Impressive
rom the excitation region under
18 and 19 [77, 78]. The ejection
o occur not only because of their
19 that the EHD clouds move
orn. Evidently the phonon flux
ısiderable importance. However,
the end of the excitation pulse.
hermalization time the phonon
tial excitation region [79]. It is
ns with a small free-path length,
leave the generation region, but

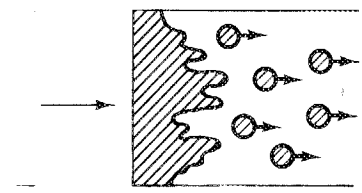

(c)

owing capillary wave instability of
f flying-away electron–hole drops.

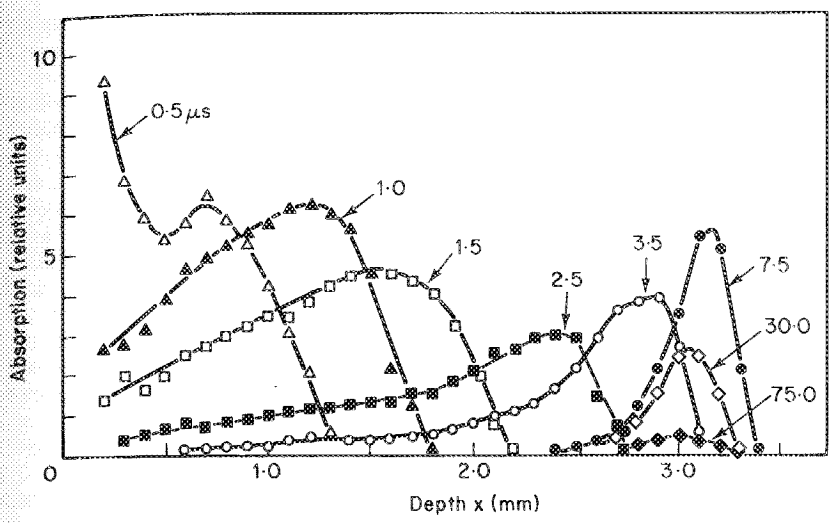

Figure 17. Positions and shapes of electron–hole drop cloud, measured by absorption of $\lambda = 3{\cdot}39\ \mu$m radiation at different delay times after a short exciting pulse [75].

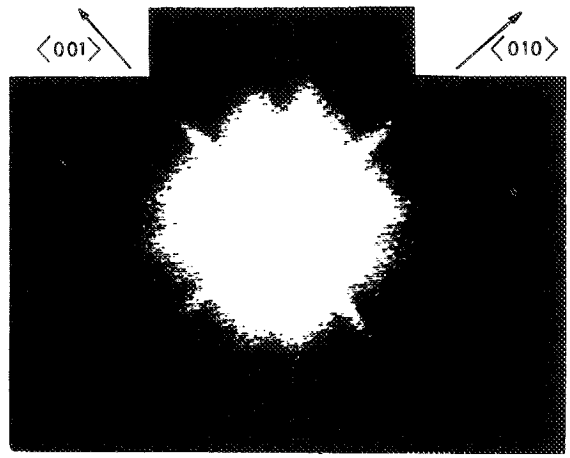

Figure 18. Anisotropic electron–hole drop cloud under conditions of stationary excitation, sharply focused at the central point of the image [77].

gradually decay and produce a phonon wind of long-wave acoustic phonons with macroscopically large mean free-paths. Such phonons interact strongly with the charge carriers.

EHD motion from the excitation region also occurs under intense stationary excitation [80, 81]. It determines the size and shape of the sample area where EHDs and the surrounding excitonic gas are dispersed, and, therefore, defines the conditions of EHD generation, growth and decay. Together with such large-scale movements in the nonequilibrium carrier system, the phonon wind changes its small-scale structure: phonon fluxes emanating from each individual EHD induce correlation in their relative position and movement, blow out excitons from the EHD neighbourhood, decrease its growth rate even at $R < R_c$, etc.

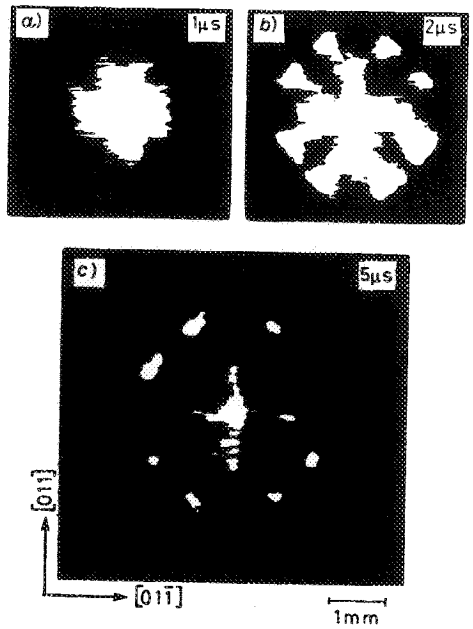

Figure 19. Time-resolved images of electron–hole droplet could after pulse excition. Delay times are shown in the right upper corners [78].

The phonon wind is only one of the manifestations of the interaction of EHD with different types of crystal deformations, static or dynamic (ultrasonic, phonons, and so on). Many other electrical, magnetic and optical phenomena, connected with the EHL, have been observed and described in reviews [1–9]. To date the EHL has been studied and understood most completely in germanium and silicon owing to the high mobility and long lifetimes of the carriers in these semiconductors. In many other semiconductors the experimental data are much scarcer. Undoubtedly the investigation of these materials will greatly increase the number of EHL manifestations and transformations in semiconductors under high excitation conditions.

References

[1] Keldysh, L. V., 1970, *Usp. fiz. Nauk*, **10**, 514.
[2] Keldysh, L. V., 1971, *Sb: Eksitony v poluprovodnikah*, edited by B. M. Vul (Moscow: Nauka), p. 5.
[3] Pokrovskii, Ya. E., 1972, *Phys. Stat. Sol.* A, **11**, 385.
[4] Voos, M., and Benoit à La Guillaume, C., 1975, *Optical Properties of Solids: New Developments*, edited by B. O. Serafin (Amsterdam: North-Holland), p. 143.
[5] Bagaev, V. S., 1975, *Springer Tracts Modern Physics Vol. 73, Excitons at High Density*, edited by H. Haken and S. Nikitine (Berlin, New York: Springer-Verlag), p. 72.
[6] Jeffries, C. D., 1975, *Science*, **89**, 955.
[7] Rice, T. M., 1977, *Solid State Physics, Vol. 32*, edited by H. Ehrenreich, F. Seitz and D. Turnball (New York, San Francisco, London: Academic Press), p. 1.
[8] Hensel, J. C., Phillips, T. G., and Thomas, G. A., 1977, *Solid State Physics, Vol. 32*, edited by H. Ehrenreich, F. Seitz and D. Turnball (New York, San Francisco, London: Academic Press), p. 88.
[9] Jeffries, C. D., and Keldysh, L. V., 1983, *Modern Problems of Condensed Matter Science Vol. 6: Electron-Hole Liquid in Semiconductors* (Amsterdam: North-Holland).
[10] Moskalenko, S. A., 1958, *Optika Spektrosk.*, **5**, 147.

[11] Lampert, M. A., 1958, *Phys. Rev. Lett.*, **1**, 450.
[12] Grun, J. B., Hönerlage, B., and Levy, R., 1982, *Modern Problems in Condensed Matter Sciences, Vol. 2: Excitons*, edited by R. I. Rashba and M. D. Sturge (Amsterdam: North-Holland), Chap. 11, p. 459.
[13] Timofeev, V. B., 1982, *Modern Problems in Condensed Matter Sciences, Vol. 2: Excitons*, edited by E. I. Rashba and M. D. Sturge (Amsterdam: North-Holland), Chap. 9, p. 349.
[14] Keldysh, L. V., 1968, *Proceedings of the Ninth International Conference on Semiconductors* (Moscow: Nauka), p. 1303.
[15] Landau, L. D., and Lifshits, E. M., 1975, *Teoreticheskaya fizika, Vol. 5, Statisticheskaya fizika*, Chap. 1 (Moscow: Nauka).
[16] Care, C. M., and March, M. H., 1975, *Adv. Phys.*, **24**, 101.
[17] Bagaev, V. E., Galkina, T. I., Gogolin, O. V., and Keldysh, L. V., 1969, *Pis'ma ZhETF*, **10**, 309.
[18] Kirczenov, G., and Singwi, K. S., 1979, *Phys. Rev.* B, **20**, 4171.
[19] Brinkman, W. F., and Rice, T. M., 1973, *Phys. Rev.* B, **7**, 1508.
[20] Keldysh, L. V., and Kopaev, Yu. V., 1964, *Fizika tverd. Tela*, **6**, 2791.
[21] Des Cloizeaux, J., 1965, *J. Phys. Chem. Solids*, **26**, 259.
[22] Halperin, B. I., and Rice, T. M., 1968, *Solid St. Phys.*, **21**, 115.
[23] Brinkman, W. F., Rice, T. M., Anderson, P. W., and Chui, S.-T., 1972, *Phys. Rev. Lett.*, **28**, 961.
[24] Combescot, M., and Nozieres, P., 1972, *J. Phys.* C, **5**, 2369.
[25] Vashishta, P., Bhattacharyya, P., and Singwi, K. S., 1973, *Phys. Rev. Lett.*, **30**, 1284.
[26] Vashishta, P., Das, S. G., and Singwi, K. S., 1974, *Phys. Rev. Lett.*, **33**, 911.
[27] Keldysh, L. V., and Onishchenko, T. A., 1976, *Pis'ma ZhETF*, **24**, 70.
[28] Andryushyn, E. A., Babichenko, V. S., Keldysh, L. V., Onishchenko, T. A., and Silin, A. P., 1976, *Pis'ma ZhETF*, **24**, 210.
[29] Andryushyn, E. A., Keldysh, L. V., and Silin, A. P., 1977, *Zh. éksp. téor. Fiz.*, **73**, 1163.
[30] Fenton, E. W., 1968, *Phys. Rev.*, **170**, 816.
[31] Brazovskii, S. A., 1972, *Zh. éksp. téor. Fiz.*, **62**, 820.
[32] Landau, L. D., and Zel'dovich, Ya. B., 1943, *Acta Phys. Chem. U.S.S.R.*, **18**, 194.
[33] Insepov, S. A., and Norman, G. E., 1972, *Zh. éksp. téor. Fiz.*, **62**, 2290.
[34] Rice, T. W., 1974, *Proceedings of the Twelfth International Conference on the Physics of Semiconductors, Stuttgart*, edited by M. H. Pilkuhn (Stuttgart: Teubner), p. 23.
[35] Ebeling, W., Kraeft, W. D., and Kremp, D., 1976, *Theory Bound States and Ionisation Equilibrium in Plasma and Solids. Vol. 5*, edited by R. Rompe and M. Steenback (Berlin: Academie-Verlag).
[36] Mott, N. F., 1961, *Phil. Mag.*, **62**, 287.
[37] Keldysh, L. V., and Silin, A. P., 1975, *Zh. éksp. téor. Fiz.*, **69**, 1053.
[38] Beni, G., and Rice, T. M., 1976, *Phys. Rev. Lett.*, **37**, 874.
[39] Rossler, M., and Zimmerman, R., 1977, *Phys. Stat. Sol.* (b), **83**, 85.
[40] Muller, G. O., and Zimmerman, R., 1979, *Physics of Semiconductors: Proceedings of the Fourteenth International Conference on the Physics of Semiconductors* (Edinburgh: SUSSP).
[41] Pokrovskii, Ya. E., and Svistunova, K. I., 1969, *Pis'ma ZhETF*, **9**, 435; Pokrovskii, Ya. E., and Svistunova, K. I., 1970, *FTP*, **4**, 491.
[42] Thomas, G. A., Frova, A., Hensel, J. C., Miller, R. E., and Lee, P. A., 1969, *Phys. Rev. B*, **13**, 1692.
[43] Thomas, G. A., Rice, T. W., and Hensel, J. C., 1974, *Phys. Rev. Lett.*, **33**, 219.
[44] Dite, A. F., Kulakovsky, V. D., and Timofeev, V. B., 1977, *Zh. éksp. téor. Fiz.*, **72**, 1156.
[45] Wolfe, J. P., Hanson, W. L., Haller, E. E., Markiewicz, R. S., Kittel, C., and Jeffries, C. D., 1975, *Phys. Rev. Lett.*, **34**, 1291.
[46] Manenkov, A. A., Miljaev, V. A., Mihilova, G. N., Sanina, V. A., and Seferov, A. S., 1976, *Z. éksp. téor. Fiz.*, **70**, 695.
[47] Bagaev, V. S., Galkina, T. I., Penin, N. A., Stopachinsky, V. B., and Churaeva, M. A., 1972, *Pis'ma ZhETF*, **16**, 120.
[48] Keldysh, L. V., and Silin, A. P., 1973, *Fizika tverd. Tela*, **15**, 1532.
[49] Stormer, H. L., and Martin, R. W., 1979, *Phys. Rev.* B, **20**, 4213.
[50] Vavilov, V. S., Zayats, V. A., and Murzin, V. N., 1969, *Pis'ma ZhETF*, **10**, 304.
[51] Markievich, R. S., Wolfe, J. P., and Jeffries, C. D., 1974, *Phys. Rev. Lett.*, **32**, 1357.

[52] KAMINSKII, A. S., POKROVSKII, Y. E., and ZHIDKOV, A. E., 1977, *Z. éksp. terr. Fiz.*, **72**, 1960.
[53] BAGAEV, V. S., ZAMKOVETS, N. V., KELDYSH, L. V., SIBELDIN, N. N., and TSVETKOV, V. A., 1976, *Z. éksp. téor. Fiz.*, **70**, 1501.
[54] SILVER, R. N., 1975, *Phys. Rev.* B, **11**, 1569.
[55] SILVER, R. N., 1975, *Phys. Rev.* B, **12**, 5689.
[56] WESTERVELT, R. M., 1976, *Phys. Stat. Sol.* (*b*), **74**, 727.
[57] WESTERVELT, R. M., 1976, *Phys. Stat. Sol.* (*b*), **76**, 31.
[58] ETIENNE, B., BENOIT À LA GUILLAUME, C., and VOOS, M., 1976, *Phys. Rev.* B, **14**, 712.
[59] STAEHLI, J. L., 1976, *Phys. Stat. Sol.* (*b*), **75**, 451.
[60] LO, T. K., FELDMAN, B. J., and JEFFRIES, C. D., 1973, *Phys. Rev. Lett.*, **31**, 224.
[61] WESTERVELT, R. M., STAEHLI, J. L., and HALLER, E. E., 1978, *Phys. Stat. Sol.* (*b*), **90**, 557.
[62] WESTERVELT, R. M., CULBERTSON, J. C., and BLACK, B. S., 1979, *Phys. Rev. Lett.*, **42**, 267.
[63] KAMINSKII, A. S., and POKROVSKII, YA E., 1970, *Pis'ma ZhETF*, **11**, 381.
[64] COMBESCOT, M., and COMBESCOT, R., 1976, *Phys. Lett.* A, **56**, 228.
[65] KOCH, S., and HAUG, H., 1979, *Physics Lett.* A, **74**, 250.
[66] POKROVSKII, YA. E., and SVISTUNOVA, K. I., 1971, *Pis'ma ZhETF*, **13**, 297.
[67] SIBELDIN, N. N., BAGAEV, V. S., TSVETKOV, V. A., and PENIN, N. A., 1973, *Fizika tverd. Tela* (*Leningrad*), **15**, 177.
[68] WORLOCK, J. M., DAMEN, T. C., SHAKLEE, K. L., and GORDON, J. P., 1974, *Phys. Rev. Lett.*, **33**, 771.
[69] VOOS, M., SHAKLEE, L. K., and WORLOCK, J. M., 1974, *Phys. Rev. Lett.*, **33**, 1161.
[70] BAGAEV, V. S., ZAMKOVETS, N. V., KELDYSH, L. V., SIBELDIN, N. N., and TSEVTKOV, V. A., 1976, *Z. éksp. téor. Fiz.*, **70**, 1501.
[71] DAMEN, T. C., and WORLOCK, J. M., 1976, *Proceedings of the Third International Conference on Light Scattering in Solids, Campinas, Brazil* (Paris: Flammarion), p. 183.
[72] BAGAEV, V. S., KELDYSH, L. V., SIBELDIN, N. N., and TSEVTKOV, V. A., 1976, *Zh. éksp. téor. Fiz.*, **70**, 702.
[73] KELDYSH, L. V., 1976, *Pis'ma ZhETF*, **23**, 100.
[74] GOURLEY, P. L., and WOLFE, J. P., 1971, *Phys. Rev.* B, **14**, 5970.
[75] ZAMKOVETS, N. V., SIBELDIN, N. N., STOPACHINSKY, V. B., and TSVETKOV, V. A., 1978, *Zh. éksp. téor. Fiz.*, **74**, 1147.
[76] KAVETSKAYA, I. V., SIBELDIN, N. N., STOPACHINSKY, V. B., and TSVETKOV, V. A., 1978, *Fizika tverd. Tela*, **20**, 3608.
[77] GREENSTEIN, M., and WOLFE, J. P., 1978, *Phys. Rev. Lett.*, **41**, 715.
[78] GREENSTEIN, M., TAMOR, M. A., and WOLFE, J. P., 1983, *Solid St. Commun.*, **45**, 355.
[79] HENSEL, J. C., and DYNES, R. C., 1977, *Phys. Rev. Lett.*, **39**, 969.
[80] DOEHLER, J. MATTOS, J. C. V., and WORLOCK, J. M., 1977, *Phys. Rev. Lett.*, **38**, 726.
[81] GREENSTEIN, M., and WOLFE, J. P., 1981, *Phys. Rev.* B, **24**, 3318.